Eidgenössische Technische Hochschule Zürich
Swiss Federal Institute of Technology Zurich

Communication Technology Laboratory
Wireless Communications Group

Professor
Armin Wittneben

Master Thesis

The Use of Loaded Antennas as Scattering Relays for Post-Cellular Networks with Closely Spaced Terminals

Autumn Semester 2015

Professor: Armin Wittneben

Supervisor:
Yahia Hassan

Student:
Bernhard Gahr

Declaration of Originality

I hereby declare that the written work I have submitted entitled

Real-Time Demonstrator for ToA based Human Motion tracking System:
Localization and Self-Calibration

is original work which I alone have authored and which is written in my own words.[1]

Author(s)

Bernhard	Gahr

Student supervisor(s)

Yahia	Hassan

Supervising lecturer

Armin	Wittneben

With the signature I declare that I have been informed regarding normal academic citation rules and that I have read and understood the information on 'Citation etiquette' (`https://www.ethz.ch/content/dam/ethz/associates/students/studium/exams/files-en/plagiarism-citationetiquette.pdf`). The citation conventions usual to the discipline in question here have been respected.

The above written work may be tested electronically for plagiarism.

Place and date	Signature

[1]Co-authored work: The signatures of all authors are required. Each signature attests to the originality of the entire piece of written work in its final form.

Contents

Preface

I would like to thank Professor Wittneben for giving me the opportunity to work on this semester thesis at the Wireless Communication Group. Further, I want to thank Yahia Hassan, my supervisor, for his help and guidance throughout the thesis.

Abstract

In nowadays wireless networks there are mainly two factors witch limit the achievable transmission rates - fading and interference. When multiple-input-multiple-output MIMO systems mostly reduce the impact of fading, the problem of interference has not yet been solved satisfyingly. The most common methods to address the problem of interference are protocols based on schemes like time-division- (TDMA), frequency-division- (FDMA), or code-division multiple access (CDMA). The solution - but in the same time also the downside of those schemes - is the unique allocation of a specific time and/or frequency slot for a single user, hence the blocking of all other users. This effect appears in the pre-logarithmic disproportional factor of the achievable sum rate.

In this thesis we address the problem of interference by the use of passive relay antennas (short: passive relays), i.e. antennas with only passive, lossless impedances attached, which interact with the receiving antennas only by the effect of coupling. By the choice of the passive elements the effect of the coupling can be changed and by using multiple passive relays, the coupling can be used to increase the signal- and reduce the interference power at the receivers.

In the following, a new description of the system will be derived, which allows an easier, more elegant way of analyzing the effect of coupling. Different solver methods are analyzed and discussed in order to find an optimal choice of the relay impedances. As some of the solvers are based on the method of gradient search, the analytical gradient will be derived. For the gradient search method, a variety of initial value choices will be compared to each other. Further, the results are evaluated and compared to previously known methods.

Notations, Acronyms and Abbreviations

Symbols

$\mathbf{x}$	Vector
$\mathbf{x}[i]$ or $\mathbf{x}_i$	i-th element of vector $\mathbf{x}$
$\|\|\mathbf{x}\|\|$	2-norm of vector $\mathbf{x}$
$\|\|\mathbf{x}\|\|_p$	LP-norm of vector $\mathbf{x}$
$\mathbf{X}$	Matrix
$\mathbf{X}^T$	transpose of matrix $\mathbf{X}$
$\mathbf{X}^{-1}$	inverse of matrix $\mathbf{X}$

Indices

x, y, z	x, y, z axis

Acronyms and Abbreviations

ETH	Eidgenössische Technische Hochschule
WCG	Wireless Communicatoin Group
UWB	Ultra-Wide Band
HMT	Human Motion Tracking
CIR	Channel Impulse Response
(N)LOS	(Non) Line of Sight
DSSS	Direct-Sequence Spread Spectrum
(A,T,TD)oA	(Angle,Time,Time Difference) of Arrival
ML	Maximum Likelihood
SDP	Semidefinite Programming
CDF	Cummulative Distribution Function
PDF	Probability Density Function
RMSE	Root Mean Squared Error

List of Figures

Chapter 1

Introduction

Future wireless networks are assumed to be of higher density at the receiver side, as more and more devices with access to the internet are appearing on the market, and more and more types of devices are staffed with moduels wich are able to connect to the internet (internet of things IoT). Examples for such scenarios are cellular networks in an urban area, wireless networks in public spaces as concert halls, or seonsor networks.

Such networks mainly suffer from two rate limiting effects: fading and interference. When the effect of fading is mostly solved by MIMO-techinques, the interference is the remaining bottleneck to achieve high data rates. Current methods to overcome interference are protocals like TDMA, FDMA or CDMA. The downside of those protocals is the unique allocation of a user to a specific time or frequency slot, hence the blocking of all other users for this period. More advanced techniques use multiple antennas as in the case of fading, to achieve multiple observations of the incoming signals and therefore the ability to zeroforce the interfering signals. This, however, is only possible, if the number of antennas per receiver is larger than the number of interfering signal streams **??** - in high density networks nearly impossible, or very expensive as the size of the receiver structure grows rapidly.

In this thesis the use of passive relays, i.e. antennae with pure imaginary impedances attached is introduced. As they are placed very closely (in terms of wavelengths) around the receivers, they interact by the effect of coupling with the receivers. By the choice of the impedances, the strengh of coupling can be changed. With an increasing number of such passive relays, the coupling can be used to steer the signal towards the receiver and block the interference.

1.1 Motivation and Goals

The achievable rate of a connection pair is propotional to the signal to noise and interference ration (SINR) (**??**). In a high power region the effect of noise can be neglected as the interference is the main diminishing factor. Therefore an interference-free connection is the main goal.

As the method of using passive relays only by their coupling is a new way of adressing the problem of interference, this thesis will look more into the achievable improvements than into the feasibility of the method. To achieve the highest possible rate for any realization, the shape of the problem will be analyzed and different solver methods will be introduced and compared.

1.2 State of the Art

TBD...
Nossek Ivrlac Hassan Wittneben

1.3 Outline

In the following chapter the whole system will be described. The effect of coupling will be analyzed and the overall transfer function - from the transmitter to the receiver will be stated. All the noise sources appearing in the systems and their transfer function will be shown and derived. The transfer functions will be splitted up into smaller, simpler (sub-) functions, so that the effect of coupling and the interference can be better described and analyzed.
As one of the solver methods is gradient search, in the third chapter the analytical gradients will be derived - for the signal, the interference and the noise part. The gradient is dependent on the covariance matrix, therefore they will be derived as well for the signal, interference and noise contributions at the reciever.
Last, the different solver methods will be evaluated. The results will be compared versus the number of relays used in a setup, versus different types of placings of the relays and versus different numbers of connection pairs. Additionally theoretical limits of the setups will be derived and the results will be compared to current protocols which overcome interference (TDMA).

Chapter 2

System

In the following the system will be described. Figure 2.1 gives an overview of it. The transmitters on the left are assumed to be widely spaced, so that they experience no coupling among each other. The signals are transmittet over a spatial interference channel, therefore a transmitted signal reaches every receiver.

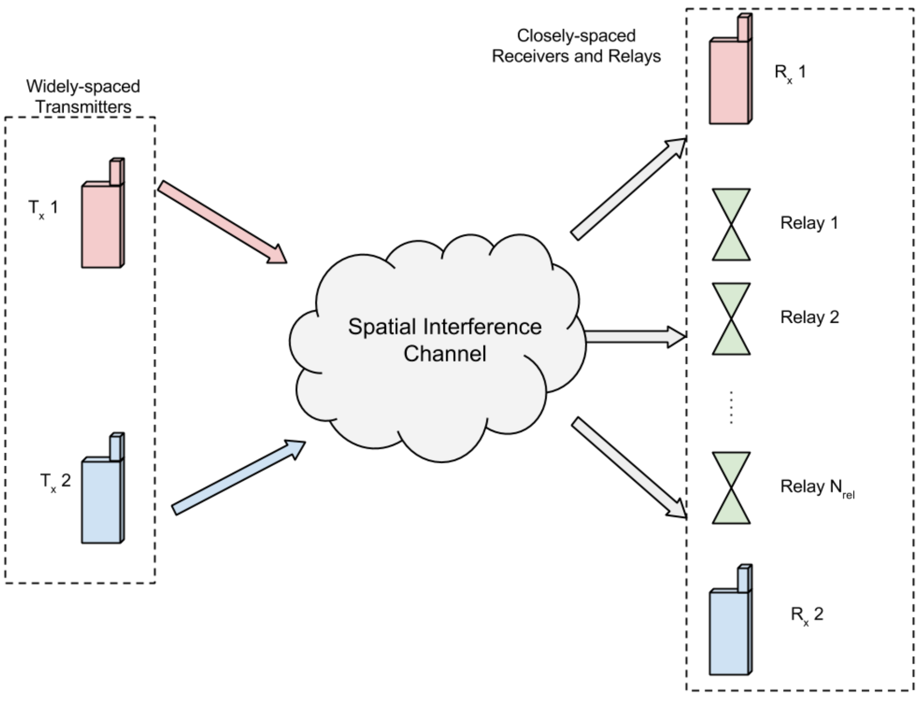

Figure 2.1: Overview of the system.

Besides the receivers, there are passive relays on the right side. The relays and the receivers are closely spaced, therefore the channels between a transmitter and the receivers and relays are spatially correlated and the elements on the receiver side experience coupling among each other.

2.1 Spatial Channel

As mentioned in the previous section the spatial channel is generated by spatial correlation among the receivers and the relays, dependent on the distance. The correlation matrix is generated by the besselfuntion according to

$$\mathbf{R}_{i,j} = B(2 \cdot d_{i,j} \cdot \pi, 0), \tag{2.1}$$

where $B(d, 0)$ is the 0-th bessel function and $d_{i,j}$ the distance between the i-th and j-th receiving element (receive antennas and relays concatenated). Therefore $\mathbf{R}$ is symmetric and 1 on its diagonal, as $B(0, 0) = 1$.

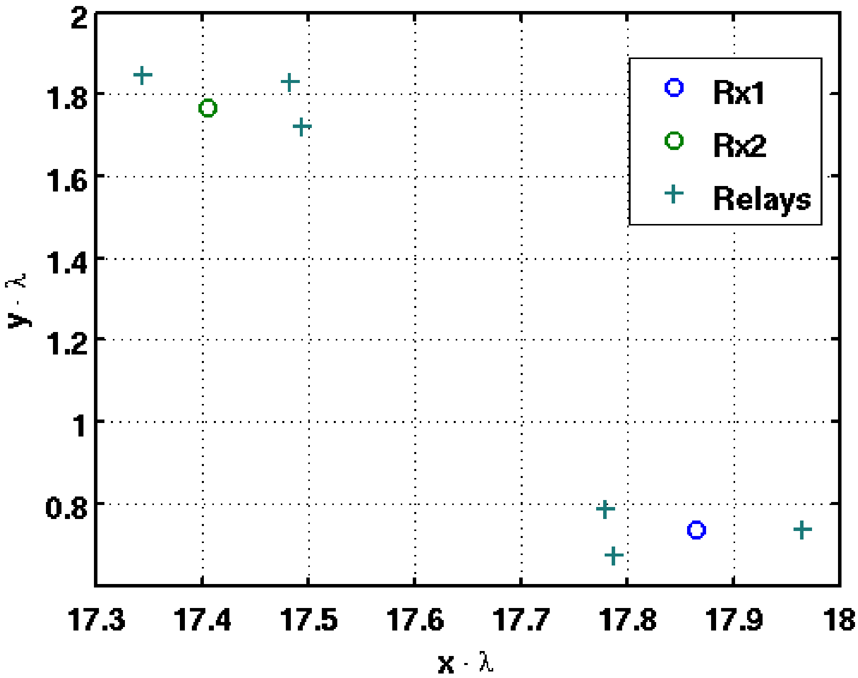

Figure 2.2: Example of the receive antenna and the relay placing.

The spatial channel from j-th transmitter to all receivers an relays is then generated by

$$\mathbf{H}_j^{\mathrm{sp}} = \mathbf{R}^{\frac{1}{2}} \cdot \mathbf{\Delta}, \tag{2.2}$$

where $\mathbf{\Delta}$ is a matrix with complex elements drawn from the standard normal distribution ($\mu = 0$ and $\sigma = 1$). Therefore $\mathbf{H}_j^{\mathrm{sp}}$ is of size $N_{\mathrm{User}} \cdot (N_{\mathrm{Rx}} + N_{\mathrm{Rel}}) \times N_{\mathrm{Tx}}$.

2.2 Receiver Circuit Description

As mentioned in Section 1.2, the idea of describing the receiver circuitry is based on the work of [1]. To do so, we represent each receiver block (shown in Figure 2.4) by n-ports. A short overview on 2-ports (simplified n-ports) is given in the following.

2.2.1 Multiport Networks

In the following a 2-port network will be analyzed. Later this can be easily extendet to a multiport network.

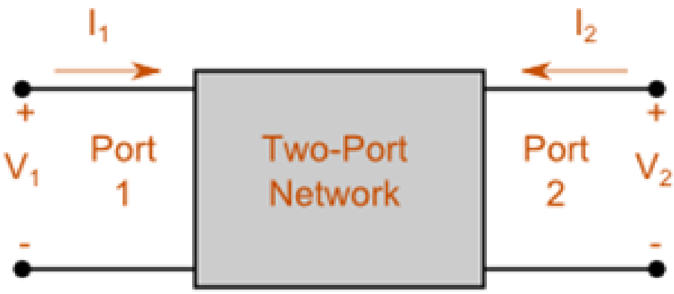

Figure 2.3: A twoport network [2].

Figure 2.3 shows a 2-port network. The twoport network can be represented by an impedance matrix $\mathbf{Z}$. The elements Z_{ij} of the matrix are defined in the following way:

$$Z_{ij} = \frac{V_i}{I_j}, \qquad (2.3)$$
$$\text{for the currents} \quad I_l = 0, \quad l \neq j.$$

Therefore the 2-port's input/output relations can be written as

$$\begin{bmatrix} V_1 \\ V_2 \end{bmatrix} = \mathbf{Z} \cdot \begin{bmatrix} I_1 \\ I_2 \end{bmatrix} \qquad (2.4)$$

For a multiport network, elements V_1, V_2, I_1 and I_2 become vectors, and the elements $Z_{ij}, \quad i, j \in \{1, 2\}$ become submatrices. Looking from the left into the network with a load R_L attached to port two, the equivalent input impedance becomes

$$\mathbf{Z}_{in_1} = \mathbf{Z}_{11} - \mathbf{Z}_{21} \cdot (\mathbf{Z}_{22} + R_L \cdot \mathbf{I})^{-1} \cdot \mathbf{Z}_{12}. \qquad (2.5)$$

With no load attached on port two, the equivalent input impedance becomes

$$\mathbf{Z}_{in_1} = \mathbf{Z}_{11}. \qquad (2.6)$$

Last, having port one short-circuited and looking from port two into the network, the equivalent network impedance becomes

$$\mathbf{Z}_{in_2} = \mathbf{Z}_{22} - \mathbf{Z}_{12} \cdot (\mathbf{Z}_{11})^{-1} \cdot \mathbf{Z}_{21}. \qquad (2.7)$$

For reciprocal (multiport-)networks (RLC-Networks, containing only passive elements), $\mathbf{Z}_{12} = \mathbf{Z}_{21}^T$.

2.2.2 Receiver Blocks

The receiver (as shown in Figure 2.4) consists of three blocks. From left to right:

1. the coupling network ($\mathbf{Z}_C$),
2. the matching network ($\mathbf{Z}_M$), and
3. the low-noise-amplifier (**LNA**).

All these blocks can be described in multiport networks. In the following each block will be discussed.

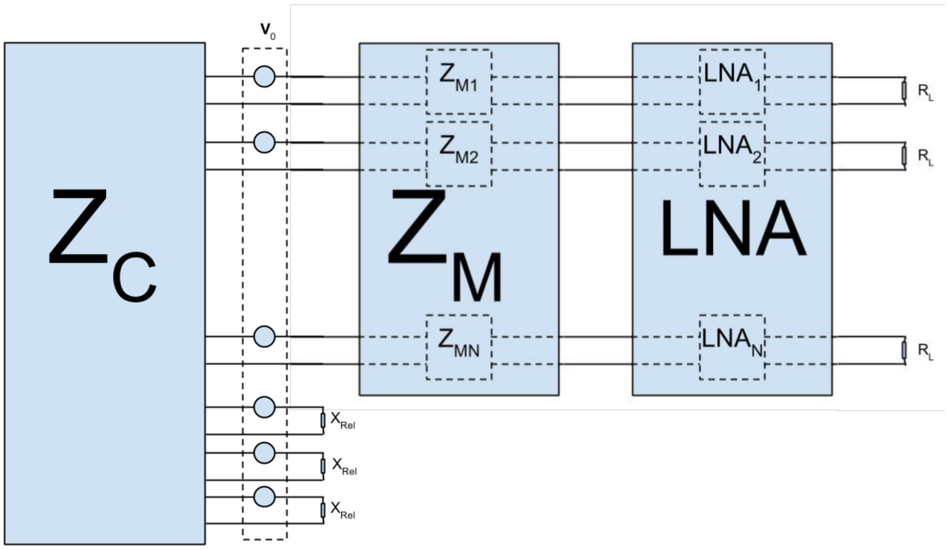

Figure 2.4: The receiver, with the coupling network $\mathbf{Z}_C$, the SP-matching network $\mathbf{Z}_M$, the LNA, and loads attached to the LNA.

The Coupling Network

The coupling network comes from the fact, that compact antenna arrays are used. The strength of the coupling between two antennas depends on the spacing between the antennas. In the following a unform spacing of the antennas is assumed. As the effect of coupling from one antenna to another is the same like the reverse, the impedance matrix $\mathbf{Z}_C$ becomes symmetric.

The Matching Network

Behind the each receiving antenna a matching network placed, to improve the performance of the receiver. For complexity and bandwith reasons ("WCNC - Paper"), single-port (SP) matching is assumed. The matching network has the form of

$$\mathbf{Z}_M = \begin{bmatrix} \mathbf{Z}_{M11} & \mathbf{Z}_{M12} \\ \mathbf{Z}_{M21} & \mathbf{Z}_{M22} \end{bmatrix}. \tag{2.8}$$

For a matching network to be lossles it must be pure imaginary and symmetric[1]. Because we assume SP matching the submatrices become diagonal, with the additional property of $\mathbf{Z}_{M12} = \mathbf{Z}_{M21}^T \implies \mathbf{Z}_{M12} = \mathbf{Z}_{M21}$.

The Low-Noise-Amplifier

In the LNA-block the received signal after the matching network gets amplified. As in the matchig network the LNA can be represented in the following way

$$\mathbf{LNA} = \begin{bmatrix} \mathbf{c} & \mathbf{d} \\ \mathbf{e} & \mathbf{g} \end{bmatrix}. \tag{2.9}$$

As each branch has it's own LNA, the submatrices $\mathbf{c}, \mathbf{e}$ and $\mathbf{g}$ are again diagonal. Additionally, matrix $\mathbf{d}$ is an all-zeros matrix if the unilateral assumtion (*the input of the LNA is not affected by the output of the LNA*) is applied.

2.2.3 Transfer Function of the Receiver

The main interest lies in the transfer function of the input voltages $\mathbf{v}_0$ to the voltage measured at the loads (in Figure 2.4) $\mathbf{v}_L$. In the following the transferfunction over each block of the receiver will be derived. We use the termination: $\mathbf{v}_i$ is the voltage on the left of the block i (i.e. v_M is the voltage on the left ports of the matching network). Additionally, we see the left ports as input ports and the right ports as output ports of each block.
For the derivation of the transferfunction we need four equivalent impedance matrices, namely

1. $\mathbf{Z}_{eqM_1}$, the impedance matrix looking from the left into the matching network,
2. $\mathbf{Z}_{eqM_2}$, the impedance matrix looking from the right into the matching network,
3. $\mathbf{Z}_{eqLNA_1}$, the impedance matrix looking from the left into the LNA, and
4. $\mathbf{Z}_{eqLNA_2}$, the impedance matrix looking from the right into the LNA.

To calculate $\mathbf{Z}_{eqM_1}$ and $\mathbf{Z}_{eqLNA_1}$, we use Equation (2.5) and get the following

$$\mathbf{Z}_{eqM_1} = \mathbf{Z}_{M11} - \mathbf{Z}_{M21} \cdot (\mathbf{Z}_{M22} + \mathbf{Z}_{eqLNA_1})^{-1} \cdot \mathbf{Z}_{M12}, \tag{2.10}$$
$$\mathbf{Z}_{eqLNA_1} = \mathbf{c} - \mathbf{e} \cdot (R_L \mathbf{I}_{N_r} + \mathbf{g})^{-1} \cdot \mathbf{d} = \mathbf{c}. \tag{2.11}$$

As we step through the receiver blocks from left to right, we always have the parallel voltages applied to each receiver block on the left. Therefore the equivalent input impedances $\mathbf{Z}_{eqM_2}$ and $\mathbf{Z}_{eqLNA_2}$ can be derived using Equation (2.6) and lead to the following

$$\mathbf{Z}_{eqM_2} = \mathbf{Z}_{M22} - \mathbf{Z}_{M12} \cdot (\mathbf{Z}_{M11})^{-1} \cdot \mathbf{Z}_{M21}, \tag{2.12}$$
$$\mathbf{Z}_{eqLNA_2} = \mathbf{g} - \mathbf{d} \cdot (\mathbf{c})^{-1} \cdot \mathbf{e} = \mathbf{g}. \tag{2.13}$$

To get the parallel input voltage on the left of the matching network, we use the principle of a voltage divider as

$$\mathbf{v_M} = \mathbf{Z}_{eqM_1} \cdot (\mathbf{Z}_{eqM_1} + \mathbf{Z}_C)^{-1} \cdot \mathbf{v_0} \tag{2.14}$$

To transfer the voltages from the left ports to the right ports of each block we proceed for each block in the following:

1. Calculate the input currents,
2. transfer the input currents to the output voltages in series, and
3. calculate the output voltages in parallel, by a voltage divider.

For the matching network, it follows:

$$\mathbf{i_M} = \mathbf{Z}_{M11}^{-1} \cdot \mathbf{v_M}, \tag{2.15}$$
$$\mathbf{v}_{LNA_{series}} = \mathbf{Z}_{M12} \cdot \mathbf{i_M} = \mathbf{Z}_{M12}\mathbf{Z}_{M11}^{-1} \cdot \mathbf{v_M}, \tag{2.16}$$
$$\begin{aligned}\mathbf{v}_{LNA} &= \mathbf{Z}_{eqLNA_1}(\mathbf{Z}_{eqLNA_1} + \mathbf{Z}_{eqM_2})^{-1} \cdot \mathbf{v}_{LNA_{series}} \\ &= \mathbf{Z}_{eqLNA_1}(\mathbf{Z}_{eqLNA_1} + \mathbf{Z}_{eqM_2})^{-1}\mathbf{Z}_{M12}\mathbf{Z}_{M11}^{-1} \cdot \mathbf{v_M},\end{aligned} \tag{2.17}$$

and equivalent for the LNA block

$$\mathbf{v_L} = R_L \mathbf{I}_{N_R}(R_L \mathbf{I}_{N_R} + \mathbf{Z}_{LNA_2})^{-1}\mathbf{Z}_{LNA12}\mathbf{Z}_{LNA11}^{-1} \cdot \mathbf{v}_{LNA}. \tag{2.18}$$

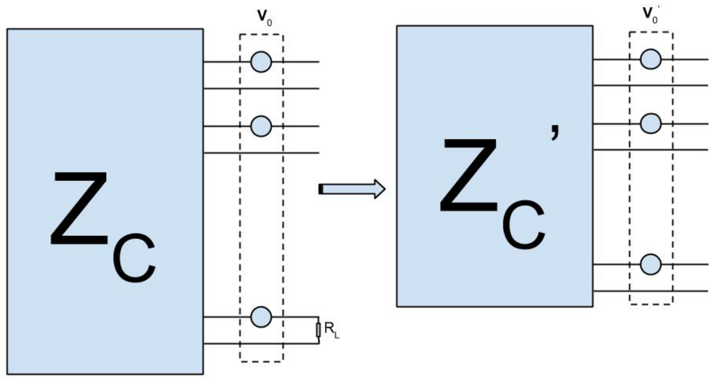

Figure 2.5: Port reduction on a network with one load connected to the last port.

Therefore we have three transfer functions to characterize our system. Denoting the transfer function form voltage $\mathbf{v}_j$ to voltage $\mathbf{v}_i$ as $\mathbf{H}_{i,j}$ (i.e. $\mathbf{v}_i = \mathbf{H}_{i,j} \cdot \mathbf{v}_j$), it follows

$$\mathbf{H}_{M,0'} = \mathbf{Z}_{eqM_1} \cdot (\mathbf{Z}_{eqM_1} + \mathbf{Z}_C)^{-1}, \tag{2.19}$$

$$\mathbf{H}_{LNA,M} = \mathbf{Z}_{eqLNA_1}(\mathbf{Z}_{eqLNA_1} + \mathbf{Z}_{eqM_2})^{-1}\mathbf{Z}_{M12}\mathbf{Z}_{M11}^{-1}, \quad \text{and} \tag{2.20}$$

$$\mathbf{H}_{L,LNA} = R_L\mathbf{I}_{N_R}(R_L\mathbf{I}_{N_R} + \mathbf{Z}_{eqLNA_2})^{-1}\mathbf{Z}_{LNA12}\mathbf{Z}_{LNA11}^{-1}. \tag{2.21}$$

And the overall transferfunction

$$\mathbf{H}_{L,0'} = \mathbf{H}_{L,LNA} \cdot \mathbf{H}_{LNA,M} \cdot \mathbf{H}_{M,0'}. \tag{2.22}$$

2.2.4 Port Reduction

In the following we describe the open circuit reduction of a system like in Figure 2.5. We do the port reduction, because we are interested in the signal only at the loads of some receivers. The signal picked up at relay antennae or not considered receivers contributes to the considered receiver by the coupling between the antennae, as described in Section 2.2.2. Passive antennas (e.g. relay antennas) can be modeled by connecting a load directly onto the coupling network as shown in Figure 2.5. Undesired receivers can be equivalently modelled, however in this case, the load corresponds to the equivalent input impedance, when looking from the left into the matching network (as in Equation (2.10)). In the following, $\mathbf{v}_C$ denotes the voltages on the ports between the coupling matrix $\mathbf{Z}_C$ and the voltage sources $\mathbf{v}_0$, the same for the currents. As we are not interested in the input/output-relation of these passive antennas, a port reduction is performed. For the port reduction, the coupling matrix $\mathbf{Z}_C$ can be represented by four submatrices

$$\mathbf{Z}_C = \begin{bmatrix} \mathbf{Z}_{OO} & \mathbf{Z}_{OL} \\ \mathbf{Z}_{LO} & \mathbf{Z}_{LL} \end{bmatrix}, \tag{2.23}$$

so that we get the system relations

$$\begin{bmatrix} \mathbf{v}_{CO} \\ \mathbf{v}_{CL} \end{bmatrix} = \begin{bmatrix} \mathbf{Z}_{OO} & \mathbf{Z}_{OL} \\ \mathbf{Z}_{LO} & \mathbf{Z}_{LL} \end{bmatrix} \cdot \begin{bmatrix} \mathbf{i}_{CO} \\ \mathbf{i}_{CL} \end{bmatrix}. \tag{2.24}$$

The index "O" denotes hereby the open circuit ports, the index "L" the ports with a load attached. The indices will change dependent on the user, however, without loss

of generality, we will derive the port reduction only for user "0" in the following. We assume, that there are N_R antennas, whereby the first Ni antennas are active (i.e. are the receive antenna of user "0"), and the later ones are passive (i.e. the antennas of the relays and of the other users,) and therefore modeled by the impedances of the relays and the input impedance of the other users' antennas. $\mathbf{Z}_{\text{pass}}$ denotes in the following the $N_r - N_i$ impedances representing the passive antennas. Therefore it is a diagonal matrix.
From Equation (2.24) and the property

$$\mathbf{v}_{CL} = \mathbf{v}_0[N_i + 1 : N_R] - \mathbf{Z}_{\text{pass}} \cdot \mathbf{i}_{CL} \quad \text{it follows,} \tag{2.25}$$

$$\mathbf{i}_{CL} = -(\mathbf{Z}_{\text{pass}} + \mathbf{Z}_{LL})^{-1}\mathbf{Z}_{LO} \cdot \mathbf{i}_{CO} - (\mathbf{Z}_{\text{pass}} + \mathbf{Z}_{LL})^{-1} \cdot \mathbf{v}_0[N_i + 1 : N_R] \tag{2.26}$$

and therefore,

$$\mathbf{v}_{CO} = (\mathbf{Z}_{OO} - \mathbf{Z}_{OL}(\mathbf{Z}_{\text{pass}} + \mathbf{Z}_{LL})^{-1}\mathbf{Z}_{LO}) \cdot \mathbf{i}_{CO} - \mathbf{Z}_{OL}(\mathbf{Z}_{\text{pass}} + \mathbf{Z}_{LL})^{-1} \cdot \mathbf{v}_0[N_i + 1 : N_R]. \tag{2.27}$$

With this port reduction the equivalent coupling matrix and input voltage for user "0" become

$$\mathbf{Z}_C^{'} = \mathbf{Z}_{OO} - \mathbf{Z}_{OL}(\mathbf{Z}_{\text{pass}} + \mathbf{Z}_{LL})^{-1}\mathbf{Z}_{LO} \quad \text{and} \tag{2.28}$$

$$\mathbf{v}_0^{'} = \mathbf{H}_0 \cdot \mathbf{H}_0^{\text{sp}} \cdot \mathbf{v_0} \tag{2.29}$$

$$\text{with} \quad \mathbf{H}_0 = \begin{bmatrix} \mathbf{I}_{N_i} & -\mathbf{Z}_{OL}(\mathbf{Z}_{\text{pass}} + \mathbf{Z}_{LL})^{-1} \end{bmatrix},$$

and so we can reduce the system shown in Figure 2.5, to the system shown in Figure 2.4.

2.2.5 Signal Covariance Matrix

To calculate the achievable sum rate of the systems (c.f. Section 2.4), we need to derive the signal covariance matrix, defined as $\mathbb{E}[\mathbf{v}_L^s \mathbf{v}_L^{s^H}]$.
We assume without loss of generality, that transmitter "0" is the corresponding partner of receiver "0". The overall transfer functions from $\mathbf{v}_0$ to $\mathbf{v}_L^s$ therefore can be extended from Equation (**??**) to

$$\mathbf{v}_L^s = \mathbf{H}_{L,LNA} \cdot \mathbf{H}_{LNA,M} \cdot \mathbf{H}_{M,0'} \cdot \mathbf{H}_0 \cdot \mathbf{H}_0^{\text{sp}} \cdot \mathbf{v}_0, \tag{2.30}$$

$$\mathbf{v}_L^s = \mathbf{H}_{L,0} \cdot \mathbf{H}_0^{\text{sp}} \cdot \mathbf{v}_0,$$

and hence the signal covariance matrix becomes

$$\mathbf{K}_{s,0} = \mathbb{E}[\mathbf{v}_L^s \mathbf{v}_L^{s^H}] = \mathbf{H}_{L,0} \cdot \mathbf{H}_0^{\text{sp}} \cdot \mathbb{E}[\mathbf{v}_0 \mathbf{v}_0^H] \cdot \mathbf{H}_0^{\text{sp}^H} \cdot \mathbf{H}_{L,0}^H, \tag{2.31}$$

where $\mathbf{H}_{L,0}$ is the transfer function including any port reduction at the receiver and $\mathbf{H}_0^{\text{sp}}$ the transferfunction over the spatial channel derived in Equation (2.2) for transmitter "0".

2.2.6 Interference Covariance Matrix

To calculate the interference covariance matrix, all the signal sources besides the partner (in this case, all but "0") have to be consider. This means, that all signal parts arriving at the loads of receiver "0" must be summed up over all the interferer. The interference covariance matrix hence becomes

$$\mathbf{K}_{i,0} = \mathbb{E}[\mathbf{v}_L^i \mathbf{v}_L^{i^H}] = \sum_{j=1}^{N_{User}-1} \mathbf{H}_{L,0} \cdot \mathbf{H}_j^{\text{sp}} \cdot \mathbb{E}[\mathbf{v}_j \mathbf{v}_j^H] \cdot \mathbf{H}_j^{\text{sp}^H} \cdot \mathbf{H}_{L,0}^H. \tag{2.32}$$

2.3 Noise Description

As mentioned in [3], there are four main noise sources in the receiver. In the following each noise source will be described and its transfer function towards the loads will be derived.

2.3.1 Antenna Noise

The antennas introduce two noise sources. The external noise $\mathbf{n}_{ext}$, collected from the radiation component of the antenna array and the noise generated by the losses in the antennas $\mathbf{n}_l$. From [4] it follows,

$$\mathbf{R}_{na} = \mathbb{E}[\mathbf{n}_{AR}\mathbf{n}_{AR}^H] = 4k_B B_W (T_{AE}\mathbb{R}\{\mathbf{Z}_{AR}\} + T_{AL}\mathbf{R}_{AR}), \tag{2.33}$$

with k_B the Boltzmann constant and B_W the bandwidth.

Transfer Function of the Antenna Noise

As the antenna noise is picked up by the antennas in the same way as the signal, the transfer function remains the same as the one derived in Equation (2.30) for the signal, e.g.

$$\mathbf{H}_{L,0} = \mathbf{H}_{L,LNA} \cdot \mathbf{H}_{LNA,M} \cdot \mathbf{H}_{M,0} \cdot \mathbf{H}_0. \tag{2.34}$$

2.3.2 LNA Noise

The LNA introduces the third noise source. From the discussion in [1], the noise of the LNA is modeled by a series of voltages and parallel currents at the input of the LNA. The noise sources have the following statistical properties,

$$\begin{aligned} \mathbb{E}[\mathbf{i}_{LNA}\mathbf{i}_{LNA}^H] &= \beta \mathbf{I}_{N_r}, \\ \mathbb{E}[\mathbf{v}_{LNA}\mathbf{v}_{LNA}^H] &= \beta R_n^2 \mathbf{I}_{N_r}, \quad \text{and} \\ \mathbb{E}[\mathbf{v}_{LNA}\mathbf{i}_{LNA}^H] &= \rho\beta R_n \mathbf{I}_{N_r}, \end{aligned} \tag{2.35}$$

with ρ and β as correlation coefficients.

Transfer Function of the LNA Noise

As written above, we have two noise sources, the serial voltage sources and the parallel current sources. First we will transfer the current source into a voltage source in series as we then can use the same transfer function for the voltage and the transferred current sources. To do so, we need the equivalent input impedances looking from the left into the LNA block and from the right into the matching network. The equivalent input impedance for the LNA network $\mathbf{Z}_{eqLNA_1}$ was already derived in (2.11). To get the equivalent input impedance for the matching network looking from the right into it we use Equation (2.5) and get

$$\tilde{\mathbf{Z}}_{eqM_2} = \mathbf{Z}_{M22} - \mathbf{Z}_{M12} \cdot (\mathbf{Z}_{M11} + \mathbf{Z}_{C'})^{-1} \cdot \mathbf{Z}_{M21}. \tag{2.36}$$

Transferring the current source into a series of voltages gives us

$$\mathbf{v}_{LNA_c} = -\tilde{\mathbf{Z}}_{eqM_2}\mathbf{i}_{LNA}, \tag{2.37}$$

and therefore a transfer function of

$$\mathbf{H}_{L,LNA_v} = R_L\mathbf{I}_{N_r}(R_L\mathbf{I}_{N_r} + \tilde{\mathbf{Z}}_{eqLNA_2})^{-1}\mathbf{e} \cdot (\mathbf{c} + \tilde{\mathbf{Z}}_{eqM_2})^{-1}, \tag{2.38}$$

for the series voltages and

$$\mathbf{H}_{L,LNA_c} = -R_L\mathbf{I}_{N_r}(R_L\mathbf{I}_{N_r} + \tilde{\mathbf{Z}}_{eqLNA_2})^{-1}\mathbf{e} \cdot (\mathbf{c} + \tilde{\mathbf{Z}}_{eqM_2})^{-1}\tilde{\mathbf{Z}}_{eqM_2}, \tag{2.39}$$

for the LNA noise currents.

2.3.3 Downstream Noise

The last noise source is the downstream noise, generated by all the circuitry after the LNA [5] and modeled by voltage sources $\tilde{\mathbf{v}}_n$ in series to the loads. With the statistical property

$$\mathbb{E}[\tilde{\mathbf{v}}_n \tilde{\mathbf{v}}_n^H] = \psi \mathbf{I}_{N_r}. \tag{2.40}$$

Transfer Function of the Downstream Noise

For the transfer function of the downstream noise we need a simple voltage divider of the loads and the equivalent input impedance $\tilde{\mathbf{Z}}_{eqLNA_2}$ looking from the right into the LNA block. Note, that this is NOT the same input impedance as in (2.13). Therefore the transfer function becomes

$$\mathbf{H}_{L,n} = R_L \mathbf{I}_{N_r} (R_L \mathbf{I}_{N_r} + \tilde{\mathbf{Z}}_{eqLNA_2})^{-1}, \tag{2.41}$$

with

$$\tilde{\mathbf{Z}}_{eqLNA_2} = \mathbf{g} - \mathbf{d} \cdot (\mathbf{c} + \tilde{\mathbf{Z}}_{eqM_2})^{-1} \cdot \mathbf{e} = \mathbf{g}, \tag{2.42}$$

whereby the unilateral assumption ($\mathbf{d} = \mathbf{0}$) was applied.

2.3.4 Noise Coupling

So far we transferred the noise from it's source to the loads behind the LNA block. However additionally to the direct path, we need to take the noise of different receiver branches into account. Therefore we transfer the noise sources to series voltages next to the antenna voltages, so that we can use the transfer functions derived in Chapter 2.2.
As in the previous Section, we consider again the four noise types. For the antenna noise, we note, that we do not need to derive a transfer function. In a first step we transfer the LNA-current noise source and the downstream noise to the LNA-voltage noise source. Therefore the LNA-current noise source is multiplied by the equivalent input impedance of the LNA

$$\mathbf{v}_{LNAc} = \mathbf{Z}_{eqLNA_1} \mathbf{i}_{LNA}. \tag{2.43}$$

For the downstream noise we note, that under the unilateral assumption, the transferred noise is zero, else

$$\mathbf{v}_{LNAn} = \mathbf{d}(\mathbf{g} + R_L \mathbf{I}_{N_R})^{-1} \tilde{\mathbf{v}}_v. \tag{2.44}$$

Now we only need to find the transfer function for the LNA-voltage source $\mathbf{v}_{LNAv}$. The transfer function over the matching network is given by

$$\mathbf{H}_{0,LNA} = \mathbf{Z}_{M12} (\mathbf{Z}_{M22} + \mathbf{Z}_{eqLNA_1})^{-1}. \tag{2.45}$$

2.3.5 Noise Covariance Matrix

As in Chapter 2.2, we will derive the noise covariance matrix. To do so, we introduce the function $\Gamma(\cdot)$, which reshapes the matrices to our needs. For example Equation (2.45) must only be applied on the noise sources of the receivers, which shall be reduced, however a multiplication of the transfer matrix with the full noise vector is desired. Let further $\Gamma(\cdot)^{-1}$, denote the function, which shapes the matrices only to the branches which are not reduced. We note the following properties

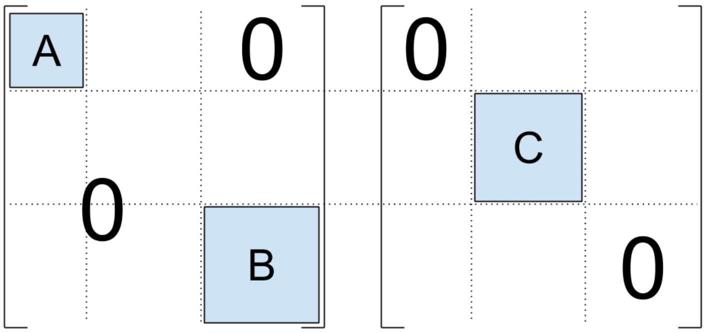

Figure 2.6: An example of the matrix shaping function. On the left the matrix shaped by $\Gamma(\cdot)$ on the right the matrix shaped by $\Gamma(\cdot)^{-1}$. The sub matrices $\mathbf{A}, \mathbf{B}$ and $\mathbf{C}$ are square matrices and lie on the diagonal.

of the function:

$$\begin{aligned} \Gamma(\mathbf{A}) \cdot \Gamma(\mathbf{B}) &= \Gamma(\mathbf{A} \cdot \mathbf{B}), \\ \Gamma(\mathbf{A}^H) &= \Gamma(\mathbf{A})^H, \\ \Gamma(\mathbf{A}) \cdot \Gamma(\mathbf{B})^{-1} &= \mathbf{0}, \quad \text{and} \\ \forall \mathbf{A}, \mathbf{B}, \quad &\text{which form a valid matrix multiplication} \quad \mathbf{A} \cdot \mathbf{B}. \end{aligned} \tag{2.46}$$

Note that the first two properties are also valid for $\Gamma(\cdot)^{-1}$. Additionally for diagonal matrices the following property holds $\Gamma(\mathbf{A}) + \Gamma(\mathbf{A})^{-1} = \mathbf{A}$.
As we have multiple noise sources, first we will describe the noise output $\mathbf{u}_L$ for each noise source, i.e.:

$$\begin{aligned} \mathbf{u}_{AR} &= \mathbf{H}_{L,0} \cdot \mathbf{n}_{AR}, \\ \mathbf{u}_{LNA_v} &= \left(\mathbf{H}_{L,0} \cdot \Gamma(\mathbf{H}_{0,LNA}) + \Gamma(\mathbf{H}_{L,LNA_v})^{-1}\right) \cdot \mathbf{v}_{LNA}, \\ \mathbf{u}_{LNA_c} &= \left(\mathbf{H}_{L,0} \cdot \Gamma(\mathbf{H}_{0,LNA}\mathbf{Z}_{eqLNA_1}) + \Gamma(\mathbf{H}_{L,LNA_c})^{-1}\right) \cdot \mathbf{i}_{LNA}, \\ \mathbf{u}_{\tilde{n}} &= \left(\mathbf{H}_{L,0} \cdot \Gamma(\mathbf{H}_{0,LNA} \cdot \mathbf{d}(\mathbf{g} + R_L \mathbf{I}_{N_R})^{-1}) + \Gamma(\mathbf{H}_{L,n})^{-1}\right) \cdot \tilde{\mathbf{v}}_n, \\ \text{and therefore} \qquad \mathbf{u}_L &= \mathbf{u}_{AR} + \mathbf{u}_{LNA_v} + \mathbf{u}_{LNA_c} + \mathbf{u}_{\tilde{n}}. \end{aligned} \tag{2.47}$$

Because all the noise sources are uncorrelated, except for the LNA noise sources (c.f. Equation (2.35)), the noice covariance matrix for user "0" can be written as:

$$\begin{aligned} \mathbf{K}_{n,0} = \mathbb{E}[\mathbf{u}_L \mathbf{u}_L^H] =& \mathbf{H}_{L,0} \mathbb{E}[\mathbf{n}_{AR} \mathbf{n}_{AR}^H] \mathbf{H}_{L,0}^H + \mathbb{E}[\mathbf{u}_{LNA_v} \mathbf{u}_{LNA_v}^H] + \mathbb{E}[\mathbf{u}_{LNA_v} \mathbf{u}_{LNA_c}^H] + \\ & \mathbb{E}[\mathbf{u}_{LNA_c} \mathbf{u}_{LNA_v}^H] + \mathbb{E}[\mathbf{u}_{LNA_c} \mathbf{u}_{LNA_c}^H] + \mathbb{E}[\mathbf{u}_{\tilde{n}} \mathbf{u}_{\tilde{n}}^H] \end{aligned} \tag{2.48}$$

For simplicity reasons, we will look in every summand seperately in the following and neglect the indices for user "0". As $-\mathbf{H}_{L,LNA_v} \cdot \tilde{\mathbf{Z}}_{eqM_2} = \mathbf{H}_{L,LNA_c}$ and using (2.33), (2.35), (2.40) and (2.46), it follows

$$\begin{aligned} \mathbf{K}_{n_{LNA_{vv}}} &= \mathbb{E}\left[\left(\mathbf{H}_{L,0} \cdot \Gamma(\mathbf{H}_{0,LNA}) + \Gamma(\mathbf{H}_{L,LNA_v})^{-1}\right) \cdot \mathbf{v}_{LNA} \mathbf{v}_{LNA}^H \cdot \right. \\ &\qquad \left. \left(\mathbf{H}_{L,0} \cdot \Gamma(\mathbf{H}_{0,LNA}) + \Gamma(\mathbf{H}_{L,LNA_v})^{-1}\right)^H\right] \\ &= \left(\mathbf{H}_{L,0} \cdot \Gamma(\mathbf{H}_{0,LNA}) + \Gamma(\mathbf{H}_{L,LNA_v})^{-1}\right) \cdot \mathbb{E}\left[\mathbf{v}_{LNA} \mathbf{v}_{LNA}^H\right] \cdot \\ &\qquad \left(\mathbf{H}_{L,0} \cdot \Gamma(\mathbf{H}_{0,LNA}) + \Gamma(\mathbf{H}_{L,LNA_v})^{-1}\right)^H \\ &= \beta R_n^2 \left(\mathbf{H}_{L,0} \cdot \Gamma\left(\mathbf{H}_{0,LNA} \mathbf{H}_{0,LNA}^H\right) \mathbf{H}_{0,LNA}^H + \Gamma\left(\mathbf{H}_{L,LNA_v} \mathbf{H}_{L,LNA_v}^H\right)^{-1}\right), \end{aligned} \tag{2.49}$$

for the LNA-voltage source and

$$\mathbf{K}_{n_{LNA_{cc}}} = \beta\Bigg(\mathbf{H}_{L,0} \cdot \Gamma\left(\mathbf{H}_{0,LNA}\mathbf{Z}_{eqLNA_1}\mathbf{Z}_{eqLNA_1}^H\mathbf{H}_{0,LNA}^H\right)\mathbf{H}_{0,LNA}^H + \Gamma\left(\mathbf{H}_{L,LNA_v}\tilde{\mathbf{Z}}_{eqM_2}\tilde{\mathbf{Z}}_{eqM_2}^H\mathbf{H}_{L,LNA_v}^H\right)^{-1}\Bigg), \tag{2.50}$$

for the LNA-current source. For the cross terms it follows

$$\begin{aligned}
\mathbf{K}_{n_{LNA_{vc}}} &= \rho\beta R_n\left(\mathbf{H}_{L,0} \cdot \Gamma\left(\mathbf{H}_{0,LNA}\mathbf{Z}_{eqLNA_1}^H\mathbf{H}_{0,LNA}^H\right)\mathbf{H}_{L,0}^H + \Gamma\left(\mathbf{H}_{L,LNA_v}\tilde{\mathbf{Z}}_{eqM_2}^H\mathbf{H}_{L,LNA_v}^H\right)^{-1}\right) \\
&\quad + \rho^*\beta R_n\left(\mathbf{H}_{L,0} \cdot \Gamma\left(\mathbf{H}_{0,LNA}\mathbf{Z}_{eqLNA_1}\mathbf{H}_{0,LNA}^H\right)\mathbf{H}_{L,0}^H + \Gamma\left(\mathbf{H}_{L,LNA_v}\tilde{\mathbf{Z}}_{eqM_2}\mathbf{H}_{L,LNA_v}^H\right)^{-1}\right) \\
&= 2\beta R_n\Bigg(\mathbf{H}_{L,0} \cdot \Gamma\left(\mathbf{H}_{0,LNA}\mathbb{R}\left\{\rho^*\mathbf{Z}_{eqLNA_1}\right\}\mathbf{H}_{0,LNA}^H\right)\mathbf{H}_{L,0}^H + \\
&\quad \Gamma\left(\mathbf{H}_{L,LNA_v}\mathbb{R}\left\{\rho^*\tilde{\mathbf{Z}}_{eqM_2}\right\}\mathbf{H}_{L,LNA_v}^H\right)^{-1}\Bigg),
\end{aligned} \tag{2.51}$$

and for the downstream noise

$$\begin{aligned}
\mathbf{K}_{n_{\tilde{n}\tilde{n}}} &= \psi\left(\mathbf{H}_{L,0} \cdot \Gamma(\mathbf{H}_{0,\tilde{n}}) + \Gamma(\mathbf{H}_{L,\tilde{n}})^{-1}\right) \cdot \left(\Gamma(\mathbf{H}_{0,\tilde{n}})^H \cdot \mathbf{H}_{L,0}^H + \Gamma(\mathbf{H}_{L,\tilde{n}}^H)^{-1}\right) \\
&= \psi\left(\mathbf{H}_{L,0} \cdot \Gamma(\mathbf{H}_{0,\tilde{n}}\mathbf{H}_{0,\tilde{n}}^H) \cdot \mathbf{H}_{L,0}^H + \Gamma(\mathbf{H}_{L,\tilde{n}}\mathbf{H}_{L,\tilde{n}}^H)^{-1}\right).
\end{aligned} \tag{2.52}$$

With these results we can form the final noise covariance matrix as

$$\mathbf{K}_{n,0} = \mathbf{H}_{L,0}\mathbb{E}[\mathbf{n}_{AR}\mathbf{n}_{AR}^H]\mathbf{H}_{L,0}^H + \mathbf{K}_{n_{LNA_{vv}}} + \mathbf{K}_{n_{LNA_{cc}}} + \mathbf{K}_{n_{LNA_{vc}}} + \mathbf{K}_{n_{\tilde{n}\tilde{n}}}. \tag{2.53}$$

2.4 Rate Calculations

2.4.1 Achievable Rate

After the derivation of the signal, interference and noise covariance matrix, we can now describe the achievable rate for each connection pair. The achievable rate for user j is described as

$$\begin{aligned}
r_j &= \log_2\left(\det\left(\mathbf{K}_{s,j}\mathbf{K}_{i,j}^{-1}\mathbf{K}_{n,j}^{-1} + \mathbf{I}_{N_r}\right)\right) \\
&= \log_2\left(\det\left(\mathbf{K}_{s,j} + \mathbf{K}_{i,j} + \mathbf{K}_{n,j}\right)\right) - \log_2\left(\det\left(\mathbf{K}_{i,j} + \mathbf{K}_{n,j}\right)\right).
\end{aligned} \tag{2.54}$$

Stacking the achievable rates per user into a vector, this leads to

$$\mathbf{r} = \begin{bmatrix} r_1 & r_2 & \cdots & r_N \end{bmatrix}^T. \tag{2.55}$$

And by this vector we can describe the achievable sum rate as

$$r_{\text{Sum}} = ||\mathbf{r}||_1, \tag{2.56}$$

with $||\cdot||_1$ the 1-norm, i.e. the sum of the elements of $\mathbf{r}$.

2.4.2 Interference Limited Rate

Another measure required in this thesis is the interference limited rate. It is calculated by only considering the signal and interference. Therefore neglecting the noise in Equation 2.54 leads to

$$r_j = \log_2\left(\det\left(\mathbf{K}_{s,j} + \mathbf{K}_{i,j}\right)\right) - \log_2\left(\det\left(\mathbf{K}_{i,j}\right)\right). \tag{2.57}$$

This is helpful, to see how good the interference was removed by the optimization, which will be introduced in Chapter 4.

2.4.3 TDMA Rate

In the later sections the results achieved in this thesis will be compared to existing protocols eliminating interference, such as TDMA. Therefore in the following the the achievable rates for the TDMA protocol will be shown.
As the time in TDMA is split up in slots in which each user is allowed to transmit without any interference, the achievable rate from Equation (2.54) reduces to the interference free achievable rate of

$$r_j = \log_2\left(\det\left(\mathbf{K}_{s,j} + \mathbf{K}_{n,j}\right)\right) - \log_2\left(\det\left(\mathbf{K}_{n,j}\right)\right). \tag{2.58}$$

It is obvious, that with no interference, this rate will be higher than the achievable rate with interference. However each user is not allowed anymore, to use the full transmission period, but only a time slot of length $\frac{1}{N_{\text{User}}} \cdot T_0$, with T_0 the length of the full transmission period. Therefore the achievable sum rate can be written as

$$\begin{aligned} r_{\text{Sum}} &= \frac{1}{N_{\text{User}}} \cdot ||\mathbf{r}||_1, \\ &= \frac{1}{N_{\text{User}}} \cdot \sum_{j=0}^{N_{\text{User}}-1} r_j. \end{aligned} \tag{2.59}$$

The term $\frac{1}{N_{\text{User}}}$ is hereby called "pre-log" factor and the reason why TDMA is not a good approach for a large number of users, as it increases linearly, however the rate per user increases only logarithmic.
There are different approaches of using TDMA, such as allowing a small number of users at the same time to transmit during one time slot. This will lead to some interference but therefore also a smaller pre-log factor. Such an approach is used in the later chapters.

Chapter 3

Analytical Gradient

In the following the derivation of the gradients will be given. In the first section the signal gradients will be derived, in the later the noise gradients. The gradients are derived to improve the achievable rates of the system (Equation (2.54)). We are interested in the gradient of the achievable rates with respect to the matching network and the passive antenna loads. Using the matrix relations from [6] the gradient becomes (neglecting the inidces for the user)

$$\frac{\partial r}{\partial \mathbf{Z}_{l,ij}} = \frac{1}{\ln(2)} \mathrm{Tr}\Bigg((\mathbf{K}_s + \mathbf{K}_i + \mathbf{K}_n)^{-1} \left(\frac{\partial \mathbf{K}_s}{\partial \mathbf{Z}_{l,ij}} + \frac{\partial \mathbf{K}_i}{\partial \mathbf{Z}_{l,ij}} + \frac{\partial \mathbf{K}_n}{\partial \mathbf{Z}_{l,ij}} \right) - (\mathbf{K}_i + \mathbf{K}_n)^{-1} \left(\frac{\partial \mathbf{K}_i}{\partial \mathbf{Z}_{l,ij}} + \frac{\partial \mathbf{K}_n}{\partial \mathbf{Z}_{l,ij}} \right) \Bigg), \tag{3.1}$$

with $l \in \{11, 12, 22, \text{pass}\}$ denoting the sub-matrices of the matching network or the passive antenna loads and i, j denoting the element in the i-th row and j-th column. In the following the gradient is split up in the signal, interference and the noise part. The derivatives for each covariance matrix will be derived.

3.1 Signal Gradient

For the signal covariance matrix, we see from Equation (2.31), that we can take the derivative of each sub transfer function and place them together afterwards by the chain rule. First of all, we check which sub transfer functions are affected by the gradient. We see that for the matching network sub matrices, we need to take the derivative of the transfer functions $\mathbf{H}_{LNA,M}$ and $\mathbf{H}_{M,0}$. For the passive antenna loads $\mathbf{Z}_{\text{pass}}$ obviously $\mathbf{H}_0$ for the port reduction is affected. Additionally $\mathbf{H}_{M,0}$ is affected because it contains $\mathbf{Z}_{C'}$.

For the following $\mathbf{J}_{ij}$ denotes the single entry matrix, with respect to the i-th row and the j-th column. If follows for the port reduction transfer function

$$\frac{\partial \mathbf{H}_0}{\partial \mathbf{Z}_{\text{pass},ij}} = \begin{bmatrix} \mathbf{0}_{N_i} & \mathbf{Z}_{OL}(\mathbf{Z}_{\text{pass}} + \mathbf{Z}_{LL})^{-1} \mathbf{J}_{ij} (\mathbf{Z}_{\text{pass}} + \mathbf{Z}_{LL})^{-1} \end{bmatrix} \tag{3.2}$$

with $\mathbf{0}_{N_i}$ the N_i by N_i all-zeros matrix. For the voltage divider before the matching network it follows,

$$\frac{\partial \mathbf{H}_{M,0}}{\partial \mathbf{Z}_{11,ij}} = \mathbf{J}_{ij}(\mathbf{Z}_{eqM_1} + \mathbf{Z}_{C'})^{-1} - \mathbf{Z}_{eqM_1}(\mathbf{Z}_{eqM_1} + \mathbf{Z}_{C'})^{-1}\mathbf{J}_{ij}(\mathbf{Z}_{eqM_1} + \mathbf{Z}_{C'})^{-1}, \tag{3.3}$$

$$\text{with} \quad \frac{\partial \mathbf{Z}_{eqM_1}}{\partial \mathbf{Z}_{M12}} = \mathbf{J}_{ij}^T(\mathbf{Z}_{M22} + \mathbf{Z}_{eqLNA_1})^{-1}\mathbf{Z}_{M12} + \mathbf{Z}_{M12}^T(\mathbf{Z}_{M22} + \mathbf{Z}_{eqLNA_1})^{-1}\mathbf{J}_{ij},$$

$$\frac{\partial \mathbf{H}_{M,0}}{\partial \mathbf{Z}_{12,ij}} = \frac{\partial \mathbf{Z}_{eqM_1}}{\partial \mathbf{Z}_{M12}}(\mathbf{Z}_{eqM_1} + \mathbf{Z}_{C'})^{-1} - \mathbf{Z}_{eqM_1}(\mathbf{Z}_{eqM_1} + \mathbf{Z}_{C'})^{-1}\frac{\partial \mathbf{Z}_{eqM_1}}{\partial \mathbf{Z}_{M12}}(\mathbf{Z}_{eqM_1} + \mathbf{Z}_{C'})^{-1}, \tag{3.4}$$

$$\text{with} \quad \frac{\partial \mathbf{Z}_{eqM_1}}{\partial \mathbf{Z}_{M22}} = \mathbf{Z}_{M12}^T(\mathbf{Z}_{M22} + \mathbf{Z}_{eqLNA_1})^{-1}\mathbf{J}_{ij}^T(\mathbf{Z}_{M22} + \mathbf{Z}_{eqLNA_1})^{-1}\mathbf{Z}_{M12},$$

$$\frac{\partial \mathbf{H}_{M,0}}{\partial \mathbf{Z}_{22,ij}} = \frac{\partial \mathbf{Z}_{eqM_1}}{\partial \mathbf{Z}_{M22}}(\mathbf{Z}_{eqM_1} + \mathbf{Z}_{C'})^{-1} - \mathbf{Z}_{eqM_1}(\mathbf{Z}_{eqM_1} + \mathbf{Z}_{C'})^{-1}\frac{\partial \mathbf{Z}_{eqM_1}}{\partial \mathbf{Z}_{M22}}(\mathbf{Z}_{eqM_1} + \mathbf{Z}_{C'})^{-1}, \tag{3.5}$$

$$\text{and with} \quad \frac{\partial \mathbf{Z}_{C'}}{\partial \mathbf{Z}_{\text{pass},ij}} = \mathbf{Z}_{OL}(\mathbf{Z}_{\text{pass}} + \mathbf{Z}_{LL})^{-1}\mathbf{J}_{ij}(\mathbf{Z}_{\text{pass}} + \mathbf{Z}_{LL})^{-1}\mathbf{Z}_{LO}$$

$$\frac{\partial \mathbf{H}_{M,0}}{\partial \mathbf{Z}_{\text{pass},ij}} = -\mathbf{Z}_{eqM_1}(\mathbf{Z}_{eqM_1} + \mathbf{Z}_{C'})^{-1}\frac{\partial \mathbf{Z}_{C'}}{\partial \mathbf{Z}_{\text{pass},ij}}(\mathbf{Z}_{eqM_1} + \mathbf{Z}_{C'})^{-1}. \tag{3.6}$$

Last, the transfer function over the matching network is affected as follows

$$\frac{\partial \mathbf{H}_{LNA,M}}{\partial \mathbf{Z}_{11,ij}} = -\mathbf{H}_{LNA,M}\mathbf{J}_{ij}\mathbf{Z}_{M11}^{-1}\mathbf{Z}_{M12}(\mathbf{Z}_{eqLNA_1} + \mathbf{Z}_{eqM_2})^{-1}\mathbf{Z}_{M12}\mathbf{Z}_{M11}^{-1} - \mathbf{H}_{LNA,M}\mathbf{J}_{ij}\mathbf{Z}_{M11}^{-1} \tag{3.7}$$

$$\begin{aligned}\frac{\partial \mathbf{H}_{LNA,M}}{\partial \mathbf{Z}_{12,ij}} = {} & \mathbf{Z}_{eqLNA_1}(\mathbf{Z}_{eqLNA_1} + \mathbf{Z}_{eqM_2})^{-1}(-\mathbf{J}_{ij}^T\mathbf{Z}_{M11}^{-1}\mathbf{Z}_{M12} - \mathbf{Z}_{M12}^T\mathbf{Z}_{M11}^{-1}\mathbf{J}_{ij})\cdot \\ & (\mathbf{Z}_{eqLNA_1} + \mathbf{Z}_{eqM_2})^{-1}\mathbf{Z}_{M12}\mathbf{Z}_{M11}^{-1} + \mathbf{Z}_{eqLNA_1}(\mathbf{Z}_{eqLNA_1} + \mathbf{Z}_{eqM_2})^{-1}\mathbf{J}_{ij}\mathbf{Z}_{M11}^{-1},\end{aligned} \tag{3.8}$$

$$\frac{\partial \mathbf{H}_{LNA,M}}{\partial \mathbf{Z}_{22,ij}} = \mathbf{Z}_{eqLNA_1}(\mathbf{Z}_{eqLNA_1} + \mathbf{Z}_{eqM_2})^{-1}\mathbf{J}_{ij}(\mathbf{Z}_{eqLNA_1} + \mathbf{Z}_{eqM_2})^{-1}\mathbf{Z}_{M12}\mathbf{Z}_{M11}^{-1} \tag{3.9}$$

With these derivations, we can apply the chain rule on the transfer function in Equation (2.30) to get

$$\begin{aligned}\frac{\partial \mathbf{K}_s}{\partial \mathbf{Z}_{l,ij}} = {} & \frac{\partial \mathbf{H}_{L,0}}{\partial \mathbf{Z}_{l,ij}} \cdot \mathbf{H}_0^{\text{sp}} \cdot \mathbb{E}[\mathbf{v}_0\mathbf{v}_0^H] \cdot \mathbf{H}_0^{\text{sp}^H} \cdot \mathbf{H}_{L,0}^H + \\ & \mathbf{H}_{L,0} \cdot \mathbf{H}_0^{\text{sp}} \cdot \mathbb{E}[\mathbf{v}_0\mathbf{v}_0^H] \cdot \mathbf{H}_0^{\text{sp}^H} \cdot \frac{\partial \mathbf{H}_{L,0}^H}{\partial \mathbf{Z}_{l,ij}}.\end{aligned} \tag{3.10}$$

3.2 Interference Gradient

As we saw in Equation (2.32), that the interference is similar to the signal, the same derivatives as in Section 3.1 will apply on the interference. Leading to the gradient of the interference covariance matrix

$$\begin{aligned}\frac{\partial \mathbf{K}_i}{\partial \mathbf{Z}_{l,ij}} = {} & \sum_{j=1}^{N_{User}-1} \frac{\partial \mathbf{H}_{L,0}}{\partial \mathbf{Z}_{l,ij}} \cdot \mathbf{H}_j^{\text{sp}} \cdot \mathbb{E}[\mathbf{v}_j\mathbf{v}_j^H] \cdot \mathbf{H}_j^{\text{sp}^H} \cdot \mathbf{H}_{L,0}^H + \\ & \sum_{j=1}^{N_{User}-1} \mathbf{H}_{L,0} \cdot \mathbf{H}_j^{\text{sp}} \cdot \mathbb{E}[\mathbf{v}_j\mathbf{v}_j^H] \cdot \mathbf{H}_j^{\text{sp}^H} \cdot \frac{\partial \mathbf{H}_{L,0}^H}{\partial \mathbf{Z}_{l,ij}}.\end{aligned} \tag{3.11}$$

3.3 Noise Gradients

As written in Section 2.3, we have four noise sources, only the two LNA noise sources correlated with each other.

3.3.1 Antenna Noise Gradient

As the antenna noise is picked up at the same place as the signal, its gradient is also the same as the signal covariance gradient. The formulas from (3.2) to (3.16) apply in the same manner to the antenna noise transfer functions. Therefore they are omitted here. We only note, that the trasfer functions $\mathbf{H}_0$, $\mathbf{H}_{M,0}$ and $\mathbf{H}_{LNA,M}$ are affected in the derivation of $\frac{\partial \mathbf{K}_n}{\partial \mathbf{Z}_{l,ij}}$, with $l \in \{11, 12, 22, \text{pass}\}$.

3.3.2 LNA Noise Gradient

Looking at the transfer function of the two LNA noise sources, we see that neither $\mathbf{H}_{L,LNA}$ nor $\mathbf{Z}_{eqLNA_1}$ are affected by the derivations. Only $\tilde{\mathbf{Z}}_{eqM_2}$ and therefore $\mathbf{H}_{L,LNA_v}$ have to be taken into account. It follows,

$$\frac{\partial \tilde{\mathbf{Z}}_{eqM_2}}{\partial \mathbf{Z}_{11,ij}} = \mathbf{Z}_{M12}(\mathbf{Z}_{M11} + \mathbf{Z}_{C'})^{-1}\mathbf{J}_{ij}(\mathbf{Z}_{M11} + \mathbf{Z}_{C'})^{-1}, \tag{3.12}$$

$$\frac{\partial \tilde{\mathbf{Z}}_{eqM_2}}{\partial \mathbf{Z}_{12,ij}} = -\mathbf{J}_{ij}(\mathbf{Z}_{M11} + \mathbf{Z}_{C'})^{-1}\mathbf{Z}_{M21} - \mathbf{Z}_{M12}(\mathbf{Z}_{M11} + \mathbf{Z}_{C'})^{-1}\mathbf{J}_{ij}^T, \tag{3.13}$$

$$\frac{\partial \tilde{\mathbf{Z}}_{eqM_2}}{\partial \mathbf{Z}_{22,ij}} = \mathbf{J}_{ij}, \tag{3.14}$$

and with $\frac{\partial \mathbf{Z}_{C'}}{\partial \mathbf{Z}_{\text{pass},ij}} = \mathbf{Z}_{OL}(\mathbf{Z}_{\text{pass}} + \mathbf{Z}_{LL})^{-1}\mathbf{J}_{ij}(\mathbf{Z}_{\text{pass}} + \mathbf{Z}_{LL})^{-1}\mathbf{Z}_{LO}$,

$$\frac{\partial \tilde{\mathbf{Z}}_{eqM_2}}{\partial \mathbf{Z}_{\text{pass},ij}} = \mathbf{Z}_{M12}(\mathbf{Z}_{M11} + \mathbf{Z}_{C'})^{-1}\frac{\partial \mathbf{Z}_{C'}}{\partial \mathbf{Z}_{\text{pass},ij}}(\mathbf{Z}_{M11} + \mathbf{Z}_{C'})^{-1}\mathbf{Z}_{M21}, \tag{3.15}$$

which results in

$$\frac{\mathbf{H}_{L,LNA_v}}{\partial \mathbf{Z}_{l,ij}} = -\mathbf{H}_{L,LNA}\mathbf{Z}_{eqLNA_1}(\mathbf{Z}_{eqLNA_1} + \tilde{\mathbf{Z}}_{eqM_2})^{-1}\frac{\partial \tilde{\mathbf{Z}}_{eqM_2}}{\partial \mathbf{Z}_{l,ij}}(\mathbf{Z}_{eqLNA_1} + \tilde{\mathbf{Z}}_{eqM_2})^{-1}. \tag{3.16}$$

3.3.3 Downstream Noise Gradient

Last, we see, that the transfer function of the downstream noise $\mathbf{H}_{L,\tilde{n}}$ is not affected by any of the derivations above under the unilateral assumption. Otherwise, $\tilde{\mathbf{Z}}_{eqLNA_2}$ is a function of the matching network and the passive antenna loads. It follows,

3.3.4 Noise Gradient

We can now write the gradient of the noise covariance matrix as

$$
\begin{aligned}
\frac{\partial \mathbf{K}_n}{\partial \mathbf{Z}_{l,ij}} = {} & \frac{\partial \mathbf{H}_{L,0}}{\partial \mathbf{Z}_{l,ij}} \mathbf{R}_{na} \mathbf{H}_{L,0}^H + \mathbf{H}_{L,0} \mathbf{R}_{na} \frac{\partial \mathbf{H}_{L,0}}{\partial \mathbf{Z}_{l,ij}}^H \\
& \frac{\partial \mathbf{H}_{L,LNA_v}}{\partial \mathbf{Z}_{l,ij}} \beta \left(R_N^2 \mathbf{I}_{N_r} - 2R_N \mathbb{R}\{\rho^* \tilde{\mathbf{Z}}_{eqM_2}\} + \tilde{\mathbf{Z}}_{eqM_2} \tilde{\mathbf{Z}}_{eqM_2}^H \right) \mathbf{H}_{L,LNA_v}^H + \\
& \mathbf{H}_{L,LNA_v} \beta \left(2R_N \frac{\partial \mathbb{R}\{\rho^* \tilde{\mathbf{Z}}_{eqM_2}\}}{\partial \mathbf{Z}_{l,ij}} + \frac{\partial \tilde{\mathbf{Z}}_{eqM_2}}{\partial \mathbf{Z}_{l,ij}} \tilde{\mathbf{Z}}_{eqM_2}^H + \tilde{\mathbf{Z}}_{eqM_2} \left(\frac{\partial \tilde{\mathbf{Z}}_{eqM_2}}{\partial \mathbf{Z}_{l,ij}} \right)^H \right) \mathbf{H}_{L,LNA_v}^H + \\
& \mathbf{H}_{L,LNA_v} \beta \left(R_N^2 \mathbf{I}_{N_r} - 2R_N \mathbb{R}\{\rho^* \tilde{\mathbf{Z}}_{eqM_2}\} + \tilde{\mathbf{Z}}_{eqM_2} \tilde{\mathbf{Z}}_{eqM_2}^H \right) \frac{\partial \mathbf{H}_{L,LNA_v}}{\partial \mathbf{Z}_{l,ij}}^H .
\end{aligned}
\tag{3.17}
$$

Chapter 4

Problem Statement and Solver Methods

In the following, the problem to optimize will be introduced an analyzed. Although the thesis is not looking into finding the optimal solution, different solver strategies have to be introduced and compared to each other, as the utility function is not trivial and the differences are severe. Their advantages and disadvantages will be shown. If not specific mentioned, we will look at a 2x2 MIMO system with one receive antenna per user and three relays, as shown in Figure 2.2. The relays in this system will be lossless, i.e. the impedances will be pure imaginary.

4.1 Utility Function

As the aim for wireless communication networks is to maximize the achievable rate, we take the formulas derived in Section 2.4, which describe the rates for each transmit-receive pair. In order to get an utility function from the achievable rates, we take the vector of achievable rates $\mathbf{r} = \begin{bmatrix} r_1 & r_2 & \cdots & r_N \end{bmatrix}^T$ from Equation (2.55). To optimize the rates, different approaches are possible.

- Optimize the minimum rate, i.e. $\max(\min(\mathbf{r}))$ (maxmin),
- Optimize the mean rate, i.e. $\max(\sum(\mathbf{r}))$ (maxsum), and
- Optimize the maximum rate, i.e. $\max(\max(\mathbf{r}))$ (maxmax).

This is done using the LP-norm ($||\mathbf{r}||_p$) [7]. By setting $p = -\text{Inf}$, the "maxmin" method is achieved. Setting $p = 1$, the "maxsum" method is applied and setting $p = +\text{Inf}$, the "maxmax" method is applied. For all values in between, the utility function "tends" to optimize the maximum and minimum value respectively.
In the following we restrict ourselves to the "maxsum" method. As the other methods easily can be applied and will lead to a similarly good result without loss of generality.

4.1.1 Convexity of the Utility Function

In the following the convexity of the utility function is analyzed. This is done, because the choice of the solver depends on the shape of the utility function (e.g. in case of a concave utility function, a normal gradient search is sufficient to provide good results).
To do so, we analyze the utility function at different input values for the passive relays. It is clear, that the function (heavily) changes for every channel realization.

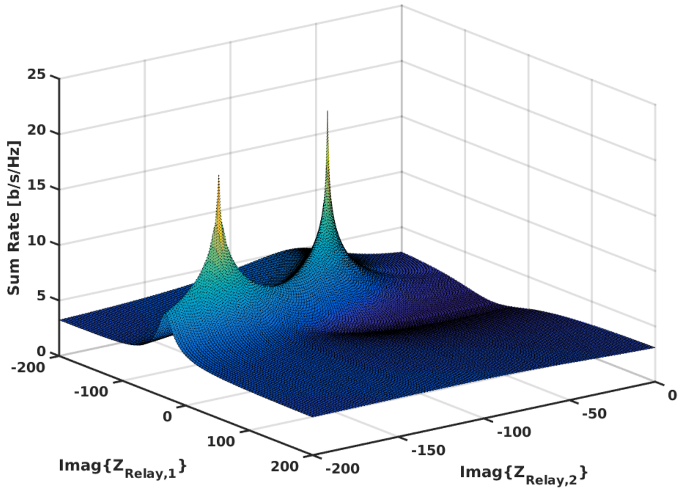

Figure 4.1: The utility function for a specific channel realization.

Figure 4.1 and 4.2 show two different channel realizations for the same input power and the same domain of two passive impedances.
For the domain of the relay values showed in Figure 4.1, even two local maxima could be found, with an immensely higher sum rate value. On the other hand, the utility function in Figure 4.2 shows only one local maximum with such a huge performance difference.

4.1.2 Dependency on the Input Power

We will analyze now the utility function for different input powers. In Figure 4.2 and Figure 4.3 we see the same channel realization for two different input powers.

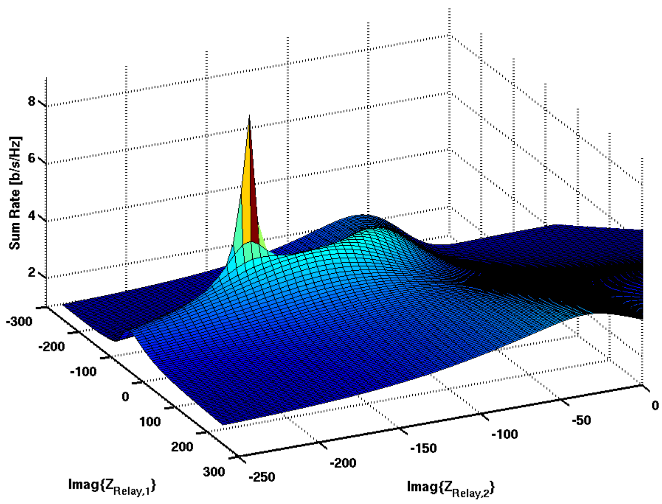

Figure 4.2: The utility function for an other specific channel realization and a high input power level.

We observe, that the optima in Figure 4.2 and Figure 4.3 lie at different impedance values of the relays, therefore we can conclude, that an optimal solution for one input power does not necessarily lead to a good solution for a different input power solution.

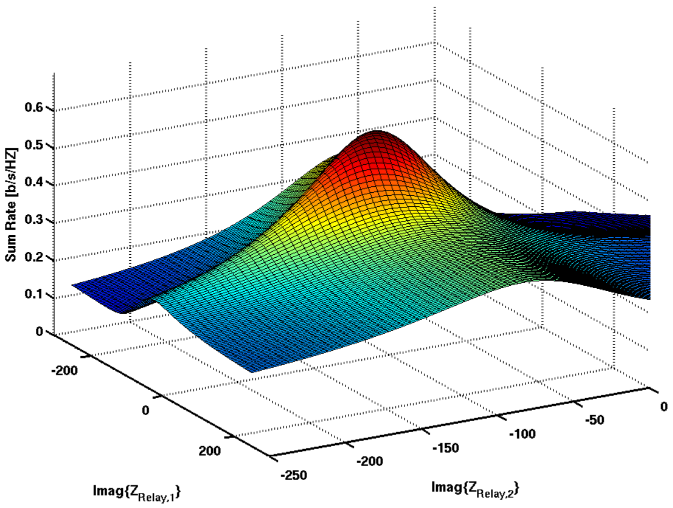

Figure 4.3: The utility function for the same specific channel realization as in Figure 4.2 and a moderate input power level.

4.1.3 Difference of Local Optima

Last, we want to look at the local optima we can possibly run into. We see in Figure 4.1, that if we hit the local optimum at the left, the performance will be nearly the same as with the local optimum at the right. However looking at Figure 4.4, we see that the difference of the global optimum of the section shown is with above 18 [b/s/Hz] severly higher than the local optimum on its left with around 8.5 [b/s/Hz]. Therefore, we can not only try to run the optimization with one initialization, but instead, we need multiple initializations, to be sure, that we haven't missed a sever maximum.

4.1.4 Complexity of the Problem

As we will discuss different solver approaches in the following Sections, a short description of the complexity of the problem is given. For each relay we use, we will have one variable (N_{Rel}), if we restrict the relays to the imaginary domain. Allowing the relay to become lossy and therefore the impedance complex, the number of variables is doubled.Further for each receiver branch, i.e. receiver antenna, we have a reciprocal (lossless) matching network (see Section 2.2.2), which has to be optimized. Therefore we have three elements per branch (in total: $3 \cdot N_{\text{R}} \cdot N_{\text{Rx}}$). For a four user MIMO system with two receive antennas and five lossy relays per user, this would lead to a problem of size $N_{\text{var}} = 2 \cdot 4 \cdot 5 + 3 \cdot 4 \cdot 2 = 64$. As mentioned in the beginning of this chapter, we look at a 2x2 MIMO system with one receive antenna and three lossless relays. The complexity of this system is therefore $N_{\text{var}} = 1 \cdot 2 \cdot 3 + 3 \cdot 2 \cdot 1 = 12$.

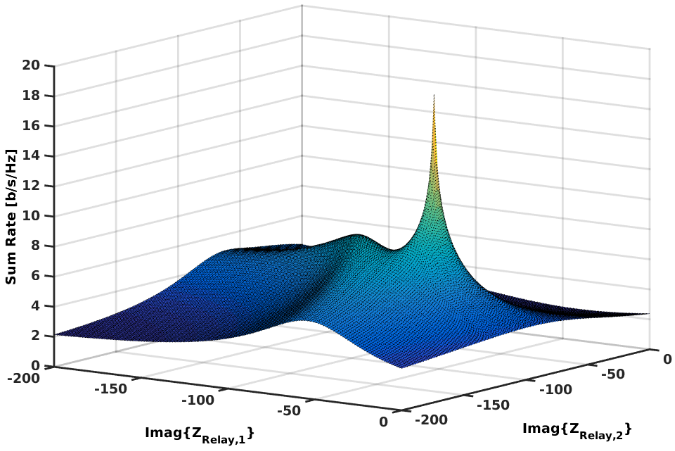

Figure 4.4: The utility function for a specific channel realization.

4.2 Gradient Search

Despite this large number of variables and the non-convexity of the utility function, the first approach remains a gradient search. Figure 4.5 shows the typical behaviour of the gradient search versus the iteration steps. In the following, different methods are described, to improve the algorithm.

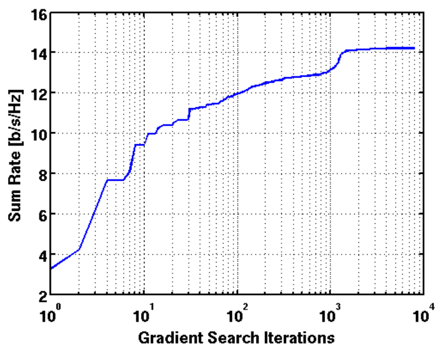

Figure 4.5: The sum rate over the gradient search iterations.

4.2.1 Choice of Initial Values

We try to overcome the non-pleasant properties of the problem with a larger number of initial guesses, so that the gradient search approach tends more towards a grid search optimization method. The gradient search routine itself is then used as a refinement step of the grid search.
Figure 4.6 shows the empirical CDFs of the optimized sum rate, for different numbers of initializations. The initial values were drawn uniformly at random for $Z_{\mathrm{Rel}}[i] \in [-600, 600]j, \quad \forall i \in [1, N_{\mathrm{Rel}}]$.
It is obvious and clear to see, that the larger the number of initializations, the better the result. However, even with 25 and 60 initializations, there improvement is still immense, which shows, that the number of initializations must be a lot larger than twice the input vector length. A good tradeoff between a decent optimization and a

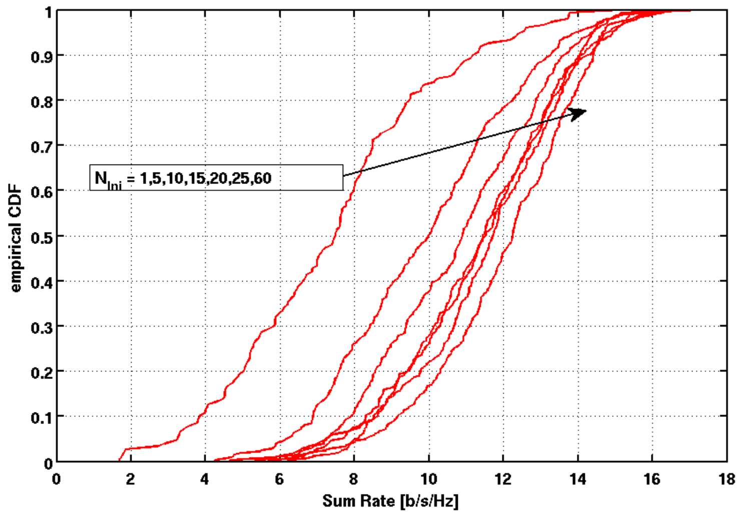

Figure 4.6: Comparison of the number of initial values used.

comparable small runtime of the optimization is achieved by a choice of four times the input vector length.

4.2.2 Adaptive Step Size

The performance of the gradient search routine is improved by the use of an adaptive step size. For each calculated gradient, the step taken into the direction of the gradient is increased until the new rate value is smaller than the previous calculated value as shown in Figure 4.7. Therefore the number of time-expensive gradient calculations is reduced immense.

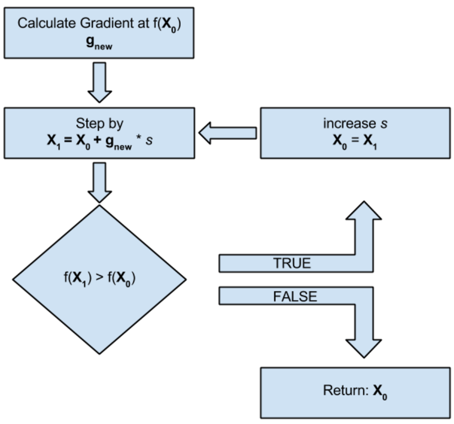

Figure 4.7: Schematic of the adaptive step size algorithm.

4.2.3 Conjugate Gradient

As the gradient search performance still requires too many iterations, further improvements were made. The shape of such complex problems can - in some cases - have the shape of a crest, where, with a unpleasant choice of the initial value, a

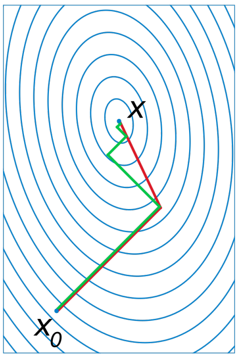

Figure 4.8: A comparison of the convergence of gradient descent with optimal step size (in green) and conjugate vector (in red) for minimizing a quadratic function associated with a given linear system[8].

pure gradient search routine might jump around the optimum, without improving a lot. Conjugate gradient routines like "Fletcher-Reeves" or "Polak-Ribière" lead to a faster convergence, as they weight the gradient by the previous gradient and a weigth factor β.
Like Polak-Ribière, the Fletcher-Reeves method updates the conjugate direction according to

$$\mathbf{s}_n = \mathbf{g}_n + \beta_n \cdot \mathbf{g}_{n-1}, \tag{4.1}$$

where $\mathbf{g}$ denotes the gradient. The conjugate direction $\mathbf{s}$ is then used to perform the conjugate gradient search. Polak-Ribière and Fletcher-Reeves differ in the way, they calculate the weight factor β.

Fletcher-Reeves

For the method of Fletcher-Reeves, β is calculated according to [9]

$$\beta_n^{FR} = \frac{\mathbf{g}_n^T \mathbf{g}_n}{\mathbf{g}_{n-1}^T \mathbf{g}_{n-1}}. \tag{4.2}$$

Polak-Ribière

For the method of Polak-Ribière, β is calculated according to [10]

$$\beta_n^{PR} = \frac{\mathbf{g}_n^T (\mathbf{g}_n - \mathbf{g}_{n-1})}{\mathbf{g}_{n-1}^T \mathbf{g}_{n-1}}. \tag{4.3}$$

In Figure 4.9 the pure gradient search (steepest ascent) method is compared to the methods of Fletcher Reeves and Polak-Ribière. The Figure shows once the optimization after 50 iterations (solid lines), to see, which method optimizes the problem the best after just a few steps, and at 500 iterations, to see which routine might get caught in the shape of the problem.
We can see, that Fletcher-Reeves is not well suited for our kind of optimization problem. Better is Polak-Ribière, which outperforms the standard gradient search method at 50 iterations and has a slightly better performance at 500 iterations.

4.3 Heuristic Optimization Algorithms

Due to the non convexity and the non trivial optimization problem, we further analyze (some) heuristic optimization methods. In the following three heuristic

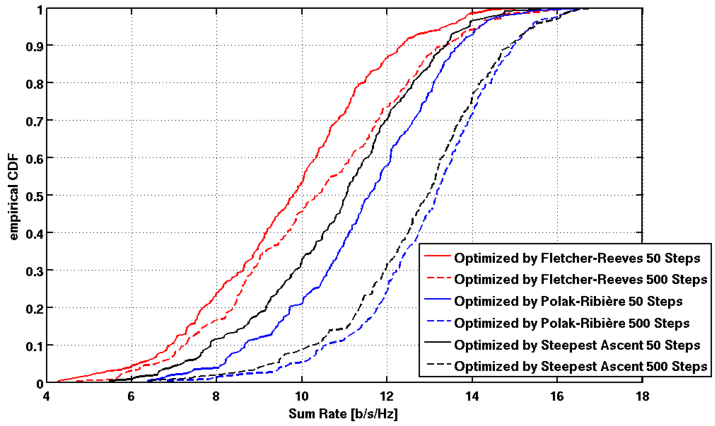

Figure 4.9: Comparison between Steepest Ascent, Polak-Ribière, and Fletcher-Reeves.

algorithms will be introduced and analyzed by their performance. They were chosen, because they already exist in the MATLAB library and do not require any strenuous implementation.

4.3.1 Simulated Annealing

Simulated Annealing was developed, as there is a deep and useful connection between statistical mechanics (the behavior of systems with many degrees of freedom in thermal equilibrium at a finite temperature) and multivariate or combinatorial optimization (finding the minimum of a given function depending on many parameters) [11]. In this thesis, Simulated Annealing was chosen as it is a method to solve optimization problems of multivariate optimization.

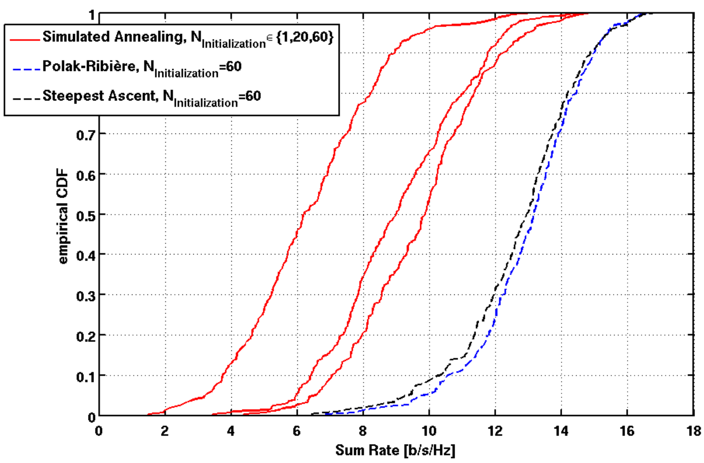

Figure 4.10: Comparison of the Simulated Annealing algorithm for different number of initializations and the results from "Polak-Ribière" and "Steepest Ascent" gradient searches.

The Algorithm used in this thesis is a build-in function of MATLAB©. A description can be found on the MathWorks homepage [12].

Figure 4.10 shows the performance of Simulated Annealing algorithm dependent on the choice of numbers of initializations (red curves). Again we see, that the more initializations we have, the better the sum rate can be optimized. However, we also see, that even with 60 initializations, Simulated Annealing leads to a result, which is worse than the sum rates achieved by steepest ascend (black dashed curve) and Polak-Ribière (blue dashed curve).

4.3.2 GlobalSearch

The other two heuristic optimization algorithms are GlobalSearch (GS) and MultiStart (MS). They are very similar to each other, the only difference is the choice of the starting values. As MultiStart requires the number of initialization values, GlobalSearch generates trial points on its own [13]. GlobalSearch - the optimization function, which we will analyze - is based on the MATLAB©built-in function *fmincon*. Figure 4.11 shows the schematics of GS and MS.

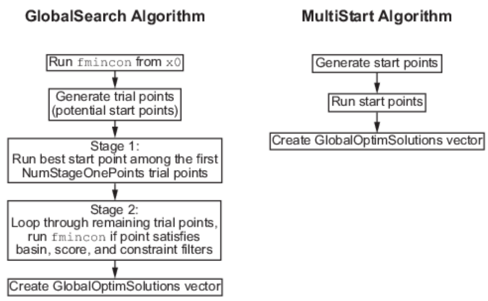

Figure 4.11: Schematics of the GlobalSearch and MultiStart algorithms [13].

Figure 4.12 shows the performance of GlobalSearch (red curve). We see, that it has almost the same performance as the conjugate gradient method by Polak-Ribière with 60 initializations (blue curve). GlobalSearch is less dependent on the initial value - for the relays it is chosen very large ($\mathbf{X}_{\mathrm{Rel}} = 1000j$) and not at random, compared to the gradient search methods, to simulate an open circuited antenna and therefore no coupling.

4.4 Further Algorithm Improvements

4.4.1 Optimization of the Interference Function

A further approach to optimize the gradient search routine is a good initial guess. The problem of the sum rate maximization is reduced only to the description of the interference. Therefore the number of variables can be reduced by a factor of two third for the matching network, as the interference function from Equation (2.28) - even after multiplication with the spatial channel transfer function (2.2) - only requires the input impedance of the matching network. This reduced problem has size of $N_{\mathrm{var}} = 2 \cdot N_{\mathrm{Rel}} + 2 \cdot N_{\mathrm{R}} \cdot N_{\mathrm{Rx}} = 2 \cdot 4 \cdot 5 + 2 \cdot 4 \cdot 2 = 56$, for the same settings as above. The factor 2 from the matching network variables comes from the fact, that with pure imaginary elements in the matching network, any complex value of the input impedance can be achieved.
Figure 4.13 shows the performance of the steepest ascent algorithm, with the pre-optimized initial values (three red dotted curves on the left). We see, that using the five best pre-optimizations leads to a performance almost as good as initializing the algorithm with 60 random vectors (red solid curve). To push the optimization even

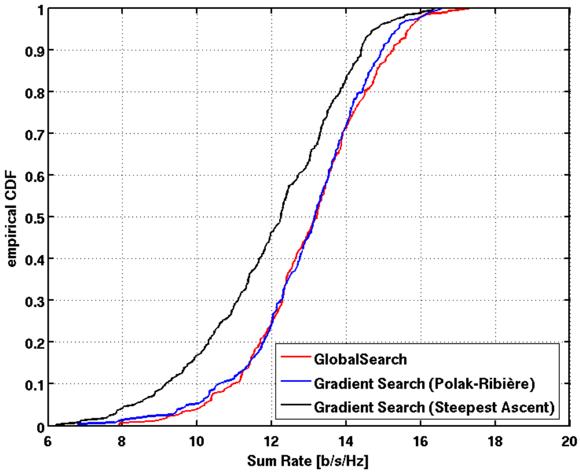

Figure 4.12: Performance of the GlobalSearch algorithm in comparison to the previous results.

further, we can combine these two techniques and take the best optimization from the five best pre-optimized initial values and 55 random initial values (red dotted curve on the right). This leads to a 0.5 [b/s/Hz] improvement at the mean and a 1.5 [b/s/Hz] improvement for the lowest 10% of the rates, than only considering random values.

Applying this to the method of Polak-Ribière (blue dotted curve), however, does not improve the results as much as with the steepest ascent method. A sum rate of only about 0.1 [b/s/Hz] higher is achieved by using pre-optimized initial values in combination with the method of Polak-Ribière.

Finally, this method is applied to the heuristic GlobalSearch routine. As mentioned in Section 4.3.2, GloablSearch is less dependent on the initial value and therefore, the initial value is chose to be open circuited for the relays. With five optimized initial values plus the standard open circuit initial value, an improvement of almost 1.0 [b/s/Hz] can be achieved (black dotted curve) compared to initializing only by the open circuited value (black solid curve).

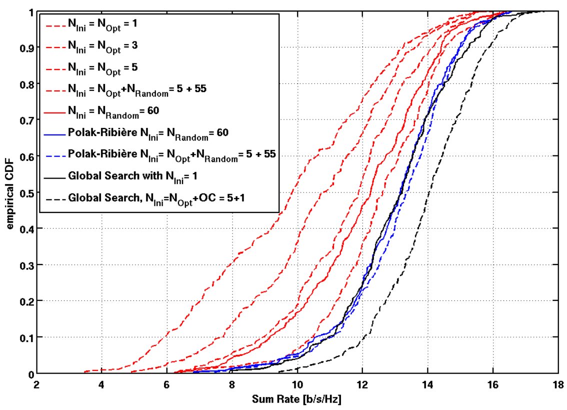

Figure 4.13: Comparison of the number of initial values used.

4.4.2 Post Refinement of GlobalSearch by Gradient Search

When the problem of gradient search is, that it may run into non optimal local maximas, the questions remaining for the heuristic solvers are: "How good are the results after all?" and "Can they be improved any further?"

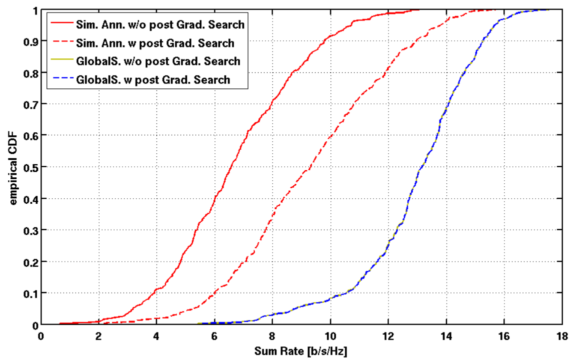

Figure 4.14: Comparison the heuristic solvers with and without a post refinement by gradient search.

The approach in finding the answers, is to use the gradient search routine on top of the heuristic solvers as a refinement. Figure 4.14 shows the performance of the Simulated Annealing and the GlobalSearch algorithm (solid red and solid yellow curves). The dashed lines show the result, when gradient search was added on top of the heuristic solvers (red for Simulated Annealing and blue for GlobalSearch). This shows, that the poor results of the Simulated Annealing algorithm does not lead to any good initial value for the gradient search as after the refinement the performance is still about 5 [b/s/Hz] worse, than the performance of GlobalSearch. Second, it shows that the performance of GlobalSearch is quite good, as any post refinement of gradient search does not lead to any significant improvement.

4.4.3 Stepwise Relay Improvements

In the previous Sections, we saw the performance of different methods for three relays per user. The number of relays was kept small for the analysis of the algorithms, so that complexity effects diminishing the performance were avoided. Increasing the number of relays might result in worse sum rates. Therefore we will have a look at the performance of the optimization and how it can be pushed in the following. For the results shown below, the number of relays were increased to seven, if not mentioned specifically.

In Figure 4.15 we see the performance of the GlobalSearch algorithm, optimizing a 2x2 MIMO system, with seven relays and one receiving antenna per user (red curve). The black curve shows the performance of the algorithm optimizing only three relays per user (c.f. red curve in Figure 4.12). Actually this should be a lower limit of the red curve, as one solution for seven relays is to optimize only three of them and open circuit the remaining four. However this is only the case for about 85% of the cases, the lowest 15% actually lead to a worse solution than only optimizing three relays. This shows, that the GlobalSeach optimization might not perform very good on larger problems, i.e. reducing the size of the problem results in a better sum rate.

Therefore one approach to prevent GlobalSearch of running into a low rate, is to reduce the number of relays to optimize and increase them stepwise. The blue curve

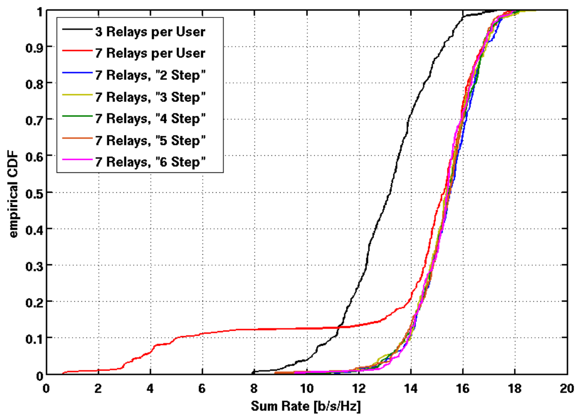

Figure 4.15: Comparison of the number of step wise optimization.

shows to result of the optimization, when GlobalSearch is allowed to optimize only two relays. Once finished, two additional relays are considered so that in total four relays per user are optimized. This is repeated until the total number of relays is reached (in this case four times, $N_{\text{Rep}} = \lceil \frac{N_{\text{Relays}}}{N_{\text{Step}}} \rceil = \lceil \frac{7}{2} \rceil = 4$). This leads to a tradeoff between the precision of the routine and the run-time, as a smaller number of relay steps (N_{Step}) will lead (most probably) to a better result, but also to a larger number of repetitions and therefore it will take a lot longer ($\approx N_{\text{Rep}} * \text{T}_0$, for T_0, the time for one optimization).

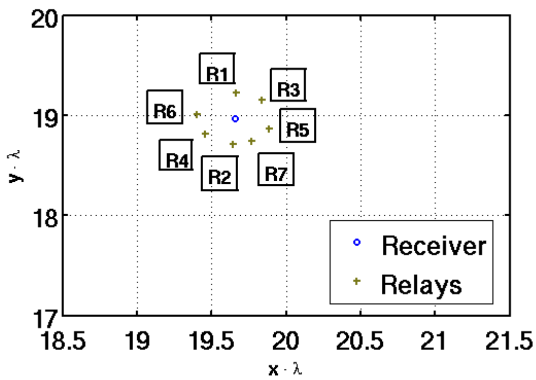

Figure 4.16: Example of choosing the relays for stepwise optimization.

The first relay is therebey chosen at random. For the following relays, the algorithm takes always the next free relay across the receiver. Figure 4.16 shows an example on how the relays would be chosen for this setting.
Back in Figure 4.15, the yellow curve shows the optimization for a stepwise increment of $N_{\text{Step}} = 3$. Therefore $N_{\text{Rep}} = 3$ had to be taken. As for $N_{\text{Step}} = 4$, $N_{\text{Step}} = 5$ and $N_{\text{Step}} = 6$ (with each $N_{\text{Rep}} = 2$), it leads almost to the same result. It can also be seen, that none of the stepwise optimized solvers has a significant low rate outlier (logarithmic scaled subplot), therefore we can say, that the outliers from the direct optimization can be avoided, when a single repetition is added.

Chapter 5

Results

In the following, the results of the thesis will be discussed. The performance of the optimization routine will be shown for different settings, i.e. for different number of relays, receiving antennas per user, users, relay placings, ... If not any further mentioned, the same settings will be used, as in Section 4, i.e. we will look at a 2x2 MIMO system with one receive antenna per user and three relays, as shown in Figure 2.2. The relays in this system will be loss less, i.e. the impedance will be pure imaginary.

5.1 Introduction of Measures for Comparison

To be able to rate the results, on how good they are, the performance will be compared to TDMA. Additionally theoretical performance limits will be shown, in order to see by how much the performance could be pushed at maximum.

5.1.1 Uncoupled Relay Rates

One of the logical performances to compare the use of loaded antennas to, is the same setting without any coupling among the relays. Logically, the "uncoupled relays rate" should be smaller than including and adapting the coupling to our needs. If no higher rate can be achieved, the whole idea of using passive relays would fail.

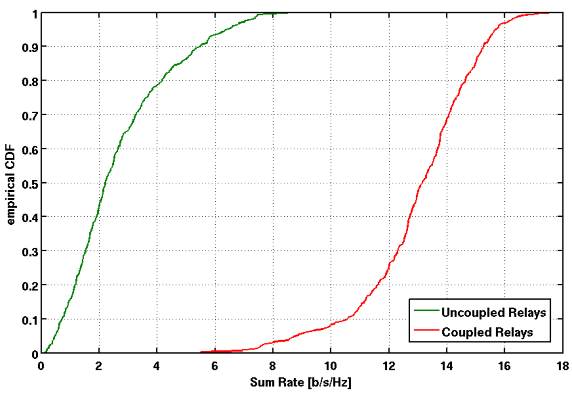

Figure 5.1: Comparison of uncoupled relays and optimized coupled relays.

In Figure 5.1, the green solid line shows the performance if no coupling among the relays and receivers exist. It is clear, that the rates including relay coupling (red solid line) are much larger than without any coupling.

5.1.2 TDMA Rates

The next performance, the optimized rates are compared to are the TDMA rates for the equivalent setup. Therefore, the relays are again assumed to be uncoupled from the receivers and the transmit/receive pairs are assumed to divide the time equally among each other for transmission.
FORMULAS (PRELOG-FACTOR)

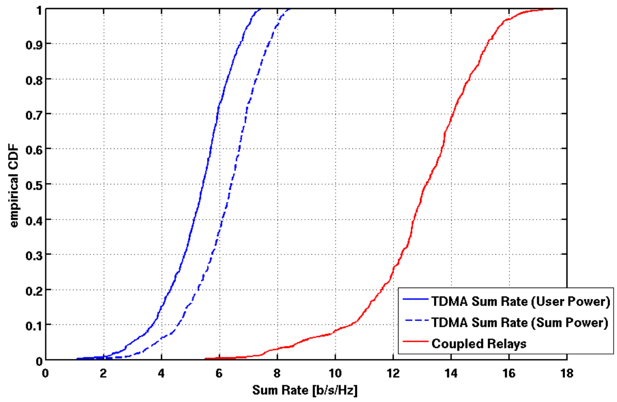

Figure 5.2: Comparison of the TDMA rate and optimized coupled relays.

In Figure 5.2, the blue solid line shows the performance if TDMA was applied under the user-power constraint (i.e. the limit of the transmit power is given per user and therefore the same for each user as in the coupled relay case) and the relays were uncoupled from the receivers. The blue dashed line shows the performance of TDMA under the sum power constraint (i.e. the limit of the transmit power is given by the total transmit power and therefore the power per user in TDMA is N_{User} times the power per user in the coupled relay case - here two times). As before, the rates including relay coupling (red solid line) are much larger than without any coupling and TDMA. Of course this comparison is more dependent on the choice of the settings (especially the choice of the number of transmit-receive pairs) and we will see different behaviors in the following sections.

5.1.3 Noise-free Rates

As we are addressing the problem of interference, a good measure is the noise-free rate (short: SIR-rate). It is calculated similar to the SINR-rate from Equation (2.54), however it only considers the interference and not the noise. As we said, in high SNR regime, the interference is the main diminishing factor for the rates (c.f. Section 2.4), the SIR-rates will give us a indicator, on how good we optimized the relays. Example curves of the SIR-rates (blue dashed lines) can be seen in Figures 5.7 to 5.9.

5.1.4 Relays as Fully Cooperation Receivers - Limit

The remaining two function to which the rates after the optimization algorithms are compared against will give limits on how good the method of loaded antennas

can be at best. The first approach is to see the relays as fully cooperation receivers, which are widely spread. Hence they experience no coupling among each other. The number of observations the receiver has on the incoming signals is increased to $N_{\mathrm{Rx}} + N_{\mathrm{Relays}}$. As we choose the number of relays larger than the number of interferer in most of the cases, this method will lead to an interference free connection.
The performance of the fully cooperation relays can be seen in Figure 5.3 (black solid curve). At median it is almost 2 [b/s/Hz] higher, than the optimized rate of the passive coupled relays. For the best 10% of the cases this is reduced to 1 [b/s/Hz] and less, for the worst 10% of the cases this lies in between 2.5 [b/s/Hz] and 4.7 [b/s/Hz].

5.1.5 Multiport Matching - Limit

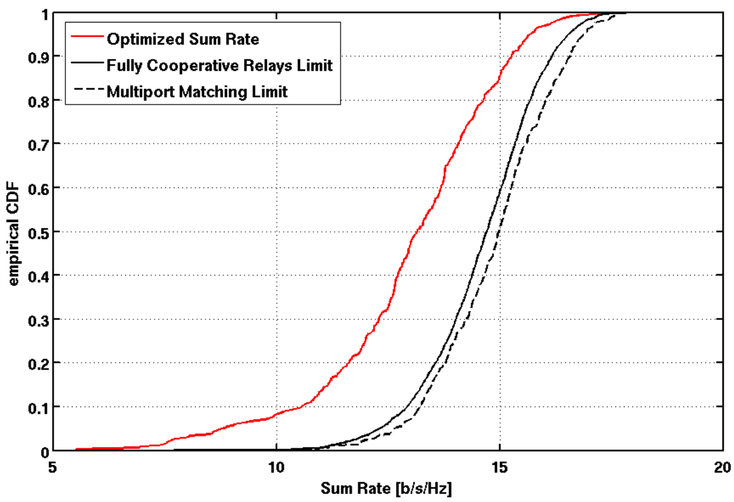

Figure 5.3: Comparison of the full cooperation relay rates, the multiport matching rate and optimized coupled relays rate.

It has been shown that the multiport matching is the optimal setting for a matching network (without considering any coupling among the receivers, and any relays) [1]. For the comparison with the coupled relays, the relays are, as in the previous section, assumed to be fully cooperating receiver antennas. However, the placing of the relays remains the same, i.e. no widely spread receivers are assumed. The number of observations one receiver has, is again $N_{\mathrm{Rx}} + N_{\mathrm{Relays}}$. And hence it can be expected, that it is higher than the optimized coupled relays rate. In Figure 5.3 and the following, this limit is shown by the black dashed line.

5.2 Relay Placing

Before analyzing the solver with different settings, the placing of the relays around a receiver is discussed a bit more in detail. Figure 5.4 shows, by which criteria, the relays were placed. The red solid circle (with radius d_z) denotes a zone around the receiver, in which no relays must not be placed. The red dashed line shows the maximum distance at which the relays may be placed away from the receiver. Within those two lines, the relays are thrown uniformly distributed. The blue circle (with radius d_{Relay}) around the relay at the right bottom denotes a zone in which no other relay may be placed, i.e. the minimum distance between each relay. If there is a violation by the relay distances, all the relays are thrown again.

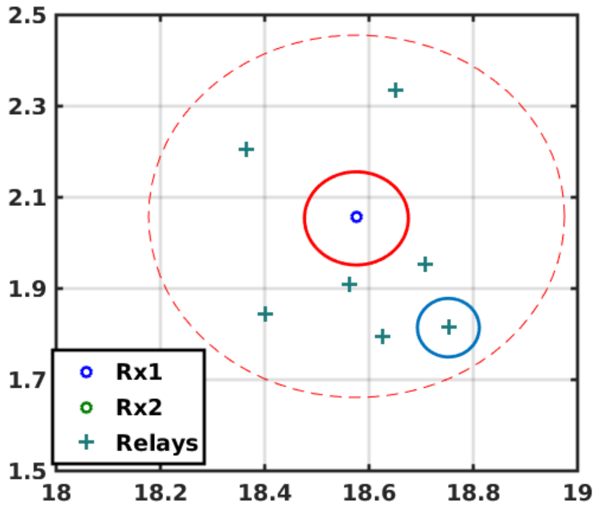

Figure 5.4: Placing the relays around a receiver uniformly distributed on a disk.

The minimum receiver distance and the minimum relay distance might differ, however, if not specially mentioned, they are assumed to be both 0.1λ. By a smaller choice of the maximum distance, the relays can be placed more dense. When the maximum distance is set equal the minimum distance, the relays will be placed on a circle around the receiver.

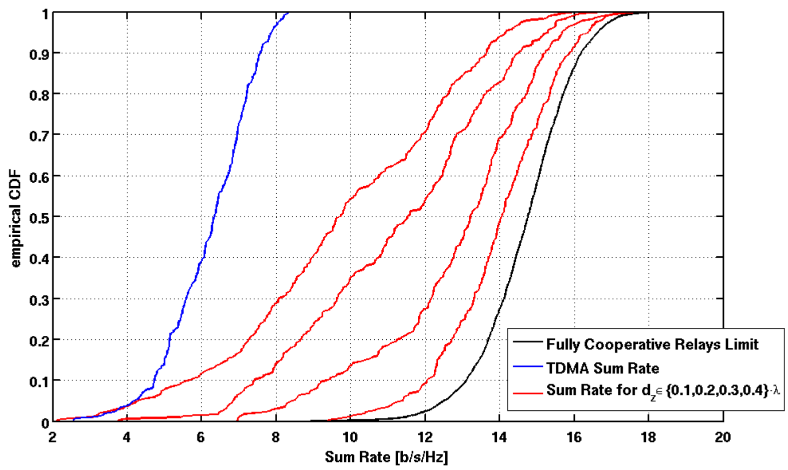

Figure 5.5: Optimized Sum Rates for different minimum distances between receiver and relays (d_z).

Figure 5.5 shows the performance of the optimized sum rate for $d_z \in \{0.1, 0.2, 0.3, 0.4\} \cdot \lambda$ (red curves from right to left). For all the curves, the relays had the same minimum spacing, i.e. $d_{\text{Relay}} = 0.1 \cdot \lambda$. Obviously a higher rate can be achieved, when the relays are closer and thus the coupling is stronger. Therefore we will use in the following $d_z = 0.1 \cdot \lambda$.

5.3 Low SNR performance

At first we want to analyze the optimization algorithm at different SNR levels. Later we will only look at a high SNR level, as our aim is to minimize the interference.

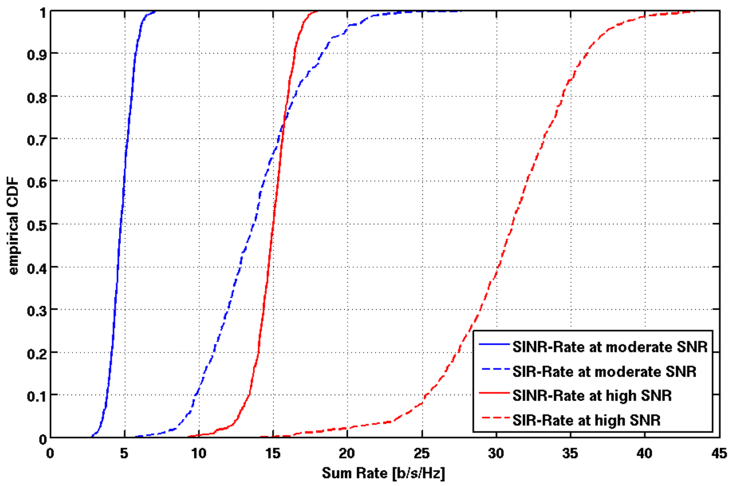

Figure 5.6: Comparison of the optimization algorithm at a moderate and high SNR level.

Figure 5.6 shows the SINR- and SIR- rates at a moderate SNR level (blue curves) and at a high SNR level (red curves). As the achievable rate at a moderate SNR level (blue solid line) is less interference driven and more noise limited, the resulting SIR-rate (blue dashed curve) is also lower than the SIR-rate of the optimized achievable rate at a high SNR region (red dashed line).
This shows for the moderate SNR level, that the optimization algorithm was matching the values of the relays and the matching network to amplify the signal and also the interference, than - like for the high SNR level - to blanket the interference.

5.4 Relays to Zero-force Interference

In the following, the number of relays required for an interference free connections will be analyzed. For the following plots, the number of receivers was set to one ($N_R = N_{R_x} = 1$) in order to increase the performance of the solver (c.f. Section 4.4.3).

5.4.1 One Interferer

To eliminate interference with two transmitter normally two observations are required. Figure 5.7 shows the performance of a transmit/receiver pair with one interferer and $N_{\mathrm{Rel}} \in \{1, 2, 3\}$ (red curves from left to right). It is clear to see, that the higher the number of relays, the better the performance of the optimized system. The blue dashed lines show the rates considering only the SI-ratio (c.f. Equation (2.57)). The use of only one relay, leads only for 10% of the cases to an

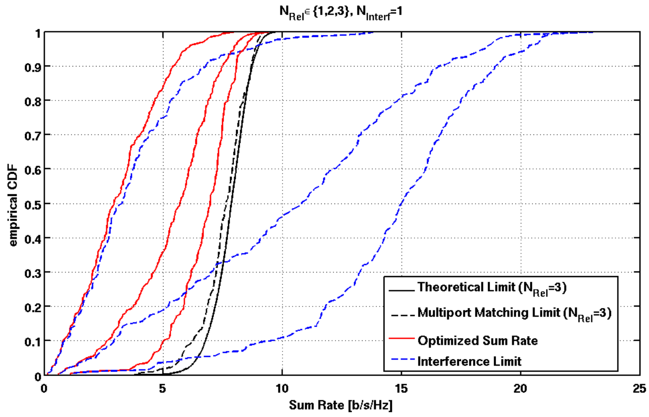

Figure 5.7: Sum rates for one interferer and one receiver with $N_{\mathrm{Rel}} \in \{1, 2, 3\}$.

interference free connection. Increasing the number of relays to two leads to an interference free connection of almost 80% of the realizations, however, to achieve for almost all realizations a noise limited connection, three relays per receiver are required.

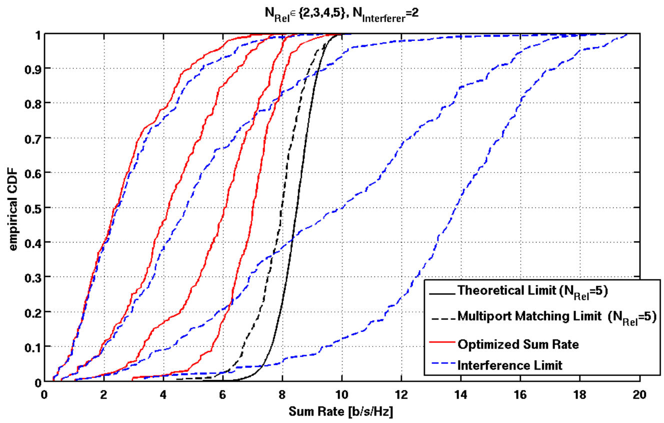

Figure 5.8: Sum rates for two interferer and one receiver with $N_{\mathrm{Rel}} \in \{2, 3, 4, 5\}$.

5.4.2 Two Interferer

To eliminate interference with three transmitter normally three observations are required. Figure 5.8 shows the performance of a transmit/receiver pair with one interferer and $N_{\mathrm{Rel}} \in \{2, 3, 4, 5\}$ (red curves from left to right). And, as before, the blue dashed lines show the rates considering only the SI-ratio.
We see, that for two relays per user, the interference limited rate behaves almost the same as the optimized achievable sum rate. For three relays per user, some realizations lead to an interference free connection. But only for five relays per user, over 90% of the realizations can be driven into an low interference state.

5.4.3 Three Interferer

To eliminate interference with four transmitter normally four observations are required. Figure 5.9 shows the performance of a transmit/receiver pair with one interferer and $N_{\text{Rel}} \in \{4,5,6,7\}$ (red and blue dashed curves from left to right).

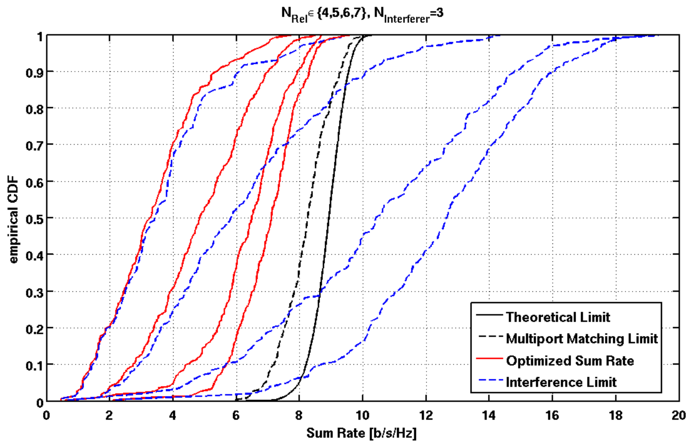

Figure 5.9: Sum rates for three interferer and one receiver with $N_{\text{Rel}} \in \{4,5,6,7\}$.

We see, that for four relays per user, the interference limited rate behaves almost the same as the optimized achievable sum rate. For five and six relays per user, some realizations lead to an interference free connection. For seven relays per user, over 90% of the realizations can be driven into an low interference state.
Comparing this to the previous results with one and two interferer, we can see, that the number of required relays to eliminate the interference grows not linearly as with the use of fully cooperating receivers. It looks like, that it requires at least twice the number of interferer ($N_{\text{Relay}} > N_{\text{Interferer}} \cdot 2$) per user, to overcome the interference.

5.5 Relay versus Rx Antenna Zeroforcing

In the following, we want to analyze what happens, if the number of relays plus receiver antennas is kept constant. First, we analyze the case of one receive/transmit pair, as this decreases the size of the problem by a factor of four. Behaviors as shown in Section 4.4.3 are therefore less likely to happen.

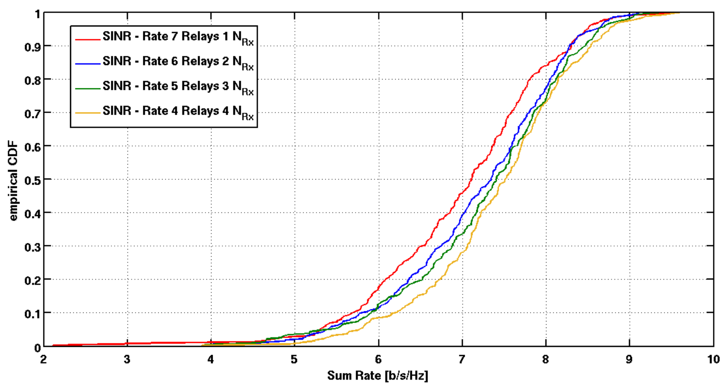

Figure 5.10: Comparison of constant $N_{\text{Relay}} + N_{\text{Rx}} = 8$, with $N_{\text{Relay}} \in \{4,5,6,7\}$ and $N_{\text{Rx}} \in \{1,2,3,4\}$.

5.5.1 One User, Three Interferer

Figure 5.10 shows the performance with three interferer and one transmit/receive pair. Obviously in the case where four receive antennas were used (yellow curve), the interference can be fully eliminated therefore it also shows the highest rate. However the performance is only 0.5 [b/s/Hz], if seven relays and only one receive antenna were used - for the values in between even less.

5.5.2 Prediction for four Users

By the results shown in the previous section, the performance of a four user system can now be predicted. A simlulation of a four user system with widely spread receivers should lead to the same results like summing up the previous curves four times.

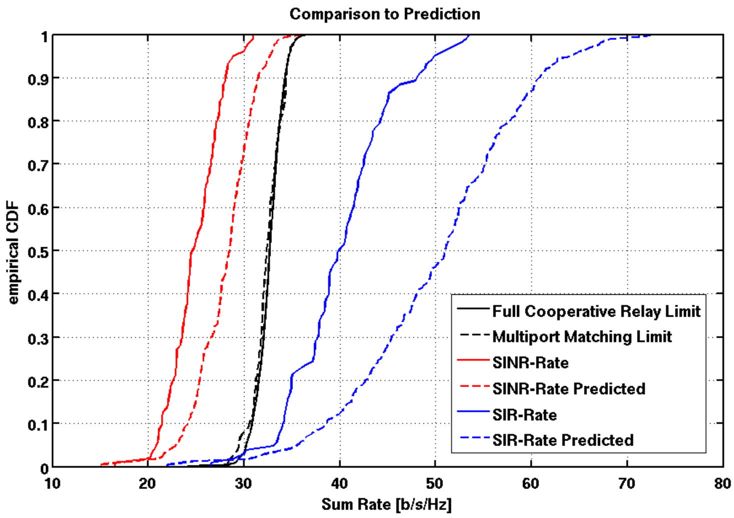

Figure 5.11: Plot of the 4 User System, with the predicted performance.

Figure 5.11 shows the predicted performance (dashed lines) compared to the simulated performance (solid lines). The rates of the simulated realizations are hereby lower than the predicted behavior. For the simulation, the receivers were not place widely spaced apart, which is one reason for the lower rates, as the coupling among the receivers is diminishing the performance. The second reason is, as mention above, a lower performance of the optimization algorithm with a larger problem. Still we can conclude, that the optimal solution must be placed between the solid and the dashed curves.
Additionally, by the black curves, theoretical limits of the sum rates are given. Because the predicted performance is not outperforming the theoretical limits, it consolidates, that the optimal solution lies around the predicted performance.

5.5.3 Four User MIMO

TO-DO: Change the following plot!

5.6 TDMA - Combination

In the following a combination of the optimization method with currently existing interference avoiding methods is analyzed. As in the previous sections, TDMA is

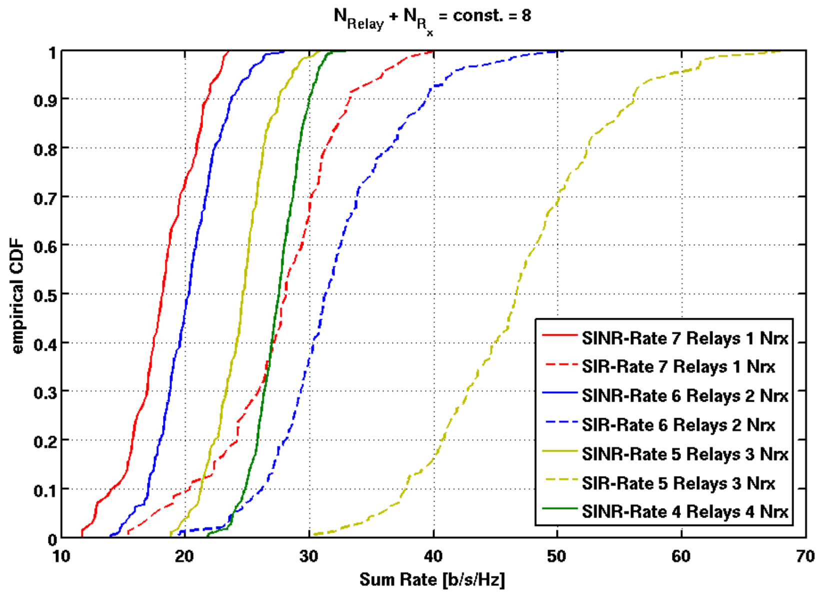

Figure 5.12: Comparison of constant $N_{\text{Relay}} + N_{\text{Rx}} = 8$, with $N_{\text{Relay}} \in \{4, 5, 6, 7\}$ and $N_{\text{Rx}} \in \{1, 2, 3, 4\}$.

used as a reference. Using two slot TDMA, reduces the number of users per slot from four to two. Therefore, the results from Figure 5.12 can be used to compare them to TDMA applied on the results from Figure 4.13.

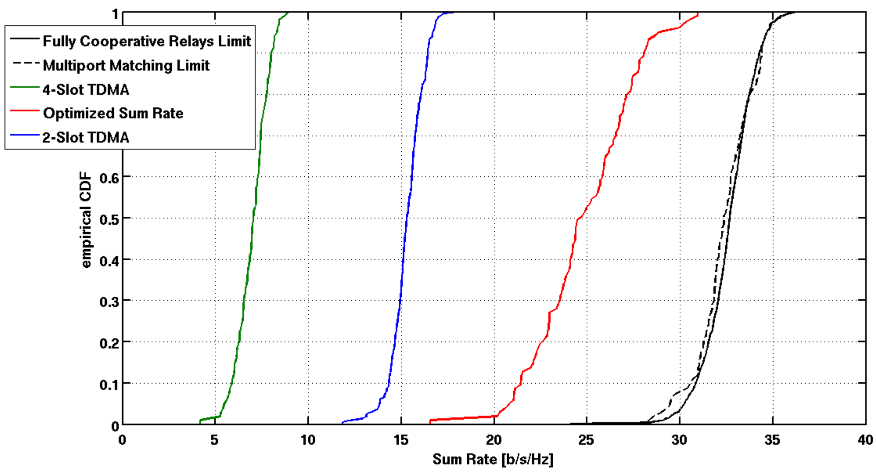

Figure 5.13: Comparison of different slot TDMA approaches.

Figure 5.13 shows in red the results of the four user MIMO system without TDMA. In blue the performance of the 2-slot TDMA approach applied on a four user system with only three relays per receiver is shown.

Chapter 6

Conclusion and Outlook

6.1 Conclusion

6.2 Future Work

Bibliography

[1] M. Ivrlac and J. Nossek, "Towards a circuit theory of communication," in *IEEE Transactions on Circuits and Systems, CAS*, July 2010.

[2] Antenna Magus, "ANTENNA MAGUS - Utilities information — The leading Antenna Design Software tool. — Antenna Design. Simplified," 2015. [Online; accessed 16-May-2015].

[3] Y. Hassan and A. Wittneben, "Rate maximization in coupled mimo systems: A generic algorithm for designing single-port matching networks," in *IEEE International Symposium on Personal, Indoor and Mobile Radio Communications, WCNC*, Sept. 2013.

[4] R. Q. Twiss, "Nyquist's and Thevenin's Theorems Generalized for Nonreciprocal Linear Networks," *Journal of Applied Physics*, vol. 26, pp. 599–602, May 1955.

[5] C. P. Domizioli and B. L. Hughes, "Front-End Design for Compact MIMO Receivers: A Communication Theory Perspective," *IEEE Transactions on Communications*, vol. 30, pp. 2938 – 2949, Oct. 2012.

[6] K. B. Petersen and M. S. Pedersen, "The Matrix Cookbook," Nov. 2012. Version 20121115.

[7] Wikipedia, "Lp space — Wikipedia, the free encyclopedia," 2015. [Online; accessed 06-May-2015].

[8] Wikipedia, "Conjugate gradient method — Wikipedia, the free encyclopedia," 2015. [Online; accessed 11-May-2015].

[9] R. Fletcher and C. M. Reeves, "Function minimization by conjugate gradients," *The Computer Journal*, vol. 7, no. 2, pp. 149–154, 1964.

[10] E. Polak and G. Ribiere, "Note sur la convergence de méthodes de directions conjuguées," *ESAIM: Mathematical Modelling and Numerical Analysis - Modélisation Mathématique et Analyse Numérique*, vol. 3, no. R1, pp. 35–43, 1969.

[11] S. Kirkpatrick, C. D. Gelatt, and M. P. Vecchi, "Optimization by simulated annealing," *SCIENCE*, vol. 220, no. 4598, pp. 671–680, 1983.

[12] The MathWorks, Inc., "How Simulated Annealing Works - MATLAB & Simulink - MathWorks Schweiz," 2015. [Online; accessed 11-May-2015].

[13] The MathWorks, Inc., "How GlobalSearch and MultiStart Work - MATLAB & Simulink - MathWorks Schweiz," 2015. [Online; accessed 11-May-2015].